1992

Crack detection with a fiber optic sensor : a parametric study of the orientation angle approach

Joram Vishlizki
Lehigh University

AUTHOR: Vishlizki, Joram

TITLE:

Crack Detectin With a Fiber Optic Sensor A Parametric Study of The Orientation Angle Approach

DATE: MAY 31, 1992

CRACK DETECTION WITH A FIBER OPTIC SENSOR

A PARAMETRIC STUDY OF THE ORIENTATION ANGLE APPROACH

by

Joram Vishlizki

A Thesis

Presented to the Graduate Committee

of Lehigh University

in Candidacy for the Degree of

Master of Science

in

Mechanical Engineering

Lehigh University

May 1992

CERTIFICATE OF APPROVAL

This thesis is accepted and approved in partial fulfillment of the requirements for master of science in Mechanical Engineering.

5/12/92
Date

Professor Richard Roberts
Thesis Advisor

Professor Robert Wei

Chairman of Department

ACKNOWLEDGEMENTS

This research was supported by the Center for Advanced Technology for Large Structural Systems (ATLSS).

The author would like to express his appreciation to his advisor, Richard Roberts, for his continuous guidance and support throughout the entire period of this research.

Thanks are also due to Professor Demitrious N. Christodoulides from the Department of Electrical Engineering, for his support on fiber optics issues.

The experiments for this research could not have been accomplished without the help of the team of the ATLSS Multidirectional Laboratory, headed by Bob Dales.

TABLE OF CONTENTS

LIST OF FIGURES

NOMENCLATURE

C_1, C_2, C_3, C_4	–	Constants of integration
D_f	–	Fiber optic diameter (inch)
E_f	–	Fiber optic modulus of elasticity (psi)
I_f	–	Fiber optic moment of inertia (inch)
Ks	–	Elastic foundation constant (psi)
L0	–	Half initial opening of a crack (inch)
L1	–	Half additional crack opening displacement (inch)
L	–	Total half opening of a crack (inch)
M	–	Bending moment (lbf–inch)
N	–	Axial force in the fiber (lbf)
P	–	Shear force working on the fiber point of symmetry (lbf)
S0	–	Trajectory of L0 in the direction of the fiber (inch)
S1	–	Trajectory of L1 in the direction of the fiber (inch)
X	–	Position along the fiber axis (inch)
Y	–	Deflection of the neutral axis of the fiber (inch)
$( )_1$	–	Index for the free section of beam model
$( )_2$	–	Index for cantilever section of beam model
$( )_{21}$	–	Index for variables affected by force P in cantilever section

NOMENCLATURE (Continued)

$( )_{22}$	–	Index for variables affected by moment M in cantilever section
Θ	–	Orientation angle between the fiber axis and the direction of crack opening propagation (radian)
σ_b	–	Bending stress (psi)

ABSTRACT

The mechanics of an optical fiber crossing a crack was investigated. It was found that the orientation angle between the direction of the crack and the fiber causes significant bending in the fiber. Parameters affecting fiber output are the orientation angle, the initial gap opening and the bonding matrix elastic foundation constant. A fiber model using a partially supported semi-infinite beam on elastic foundation was developed. Calculations with this model for a multimode optical fiber (50/125μm) and a matrix with an elastic foundation constant of 500 ksi shows that the bending stress levels are low for deflections in the order of the fiber diameter. Experiments were made to measure optical attenuation of the light passing through the bent fiber versus the orientation angle and initial gap opening. The results show an agreement with the theoretical model for stress as no failure occurred in the expected range. The sensitivity of such a sensor was found to be higher for a smaller initial gap opening and greater orientation angles. Crack detection levels were achieved when the matrix cracked and losses of 0.1 to 0.5 db were observed for strain levels of 0.6 to 6%.

1. INTRODUCTION

The use of optical fibers as sensors has been reported within the last decade for a variety of measurements such as displacement, strain and temperature [1]. The immunity of optical fibers to radio frequency interference and the ability to operate without a local power source for each sensor, suggests that Optical Fiber Sensors (OFS) will have an advantage in many practical applications.

Detection of cracks using optical fibers has also been reported in the literature [2]. One such application involves embedding the optical fiber in a brittle adhesive on the surface of structural member. When a crack forms in the structure and opens to a critical size the adhesive will fracture. The result of this failure is a break in the fiber and a loss of transmitted light, indicating a crack.

A detailed study of a fiber optic crossing a crack will lead to a better understanding of the fiber failure conditions. This will result in better control of the optical fiber output due to mechanical strain and enable sensor output in the period between the failure of the adhesive material and failure of the fiber.

An adhesive with a low strength is necessary to detect small cracks in the structural member. A low modulus of elasticity is also important to avoid

reinforcing effects on the structure before the failure of the adhesive. An adhesive failure may or may not break the fiber. In the case of failure of the optical fiber, detection of the crack is obvious. However, when the optical fiber is not broken the detection of a crack is possible if power attenuation or a change in phase of the light source is monitored.

A crack on the surface of a structural member produces high stresses and strains at the crack tips. At some point, the strains in the member will exceed the fracture strain in the adhesive. At this point, the adhesive fractures. The structural member and the adhesive are now subject to the same opening displacement (assuming the thickness of the matrix is very small relative to the structure thickness).

By choosing an adhesive with certain mechanical properties in tension (modulus of elasticity and maximum strain), the fracture limit can be controlled. This approach is similar to that in brittle coating materials [3]. Once the matrix is cracked, it is important to find conditions that keep the stress level in the fiber optic under the failure limit, to allow losses to be measured due to crack propagation.

1.1 PRINCIPLES OF OPTICAL FIBER SENSORS

1.1.1 MONOMODE AND MULTIMODE OPTICAL FIBERS

An Optical Fiber [4] consists of two concentric layers (Figure 1); An internal core and a cladding which surrounds the core.

When light from the core reaches the cladding (which has a lower refractive index) with an incident angle greater than some critical angle, the light is reflected back to the core at the same angle and then propagates along the axis of the fiber in a zigzag mode. Monomode fibers have a small core diameter and a step refractive index profile which limit its use to transmitting single mode light only. Multimode fibers have a large core diameter and a step or a graded index profile with a large acceptance angle of light entering the core, allowing many modes of light to be transmitted.

1.1.2 INTERFEROMETRIC AND INTENSITY METHODS

Interferometric and Intensity Optical Fiber Sensors (OFS) are common techniques for measuring mechanical strain and displacement [5].

Interferometric Optical Fiber Sensors are based on the fact that when two beams of light interface, the visibility of the interference fringes produced are controlled by the coherence of the light. The property of coherent light is achieved by using

monomode fibers which are preferred for interferometric applications. The use of Interferometric methods involves a light source, a beam splitter (or coupler) which divides the beam to a signal arm and a reference arm and a second coupler which superimposes the two signals to a single fiber, and a detector at the end of the single fiber.

A change in the speed of light in the signal arm results in a phase difference at the output which can be measured by resultant fringes. Changes in the speed of the light are caused by changes in length of the signal arm and/or changes in photoelastic properties of the optical fiber material (glass) due to mechanical stresses. As a result, such a sensor is sensitive to changes in the order of the wavelength being used.

The Intensity Optical Fiber Sensors technique is based on the attenuation which occurs in the fiber due to changes in the refractive index between the core and the cladding. When this index changes, some light is transmitted from the core to the cladding and is lost. Such a change in the index occurs mostly because of mechanical bending of the fiber. The result is a high sensitivity to fiber bending and an insensitivity to changes in fiber length.

The use of the intensity Optical Fiber Sensors involves a light source and a

detector. A reference arm might be used in cases where measurements are performed with reference to the power source and cannot be evaluated independently with local losses.

The O.T.D.R technique, which is discussed in the next section, combines the input power source and the detector into one unit which gives a readout of local losses. As a result, losses which are not caused by sensor outputs can be eliminated.

1.1.3 OPTICAL TIME DOMAIN REFLECTOMETER (O.T.D.R)

An O.T.D.R is a device which launches a very narrow optical pulse into the optical fiber and then measures backscatter and reflections versus time. The reflection and backscatter are detected from each point along the fiber by measuring the roundtrip time delay of returned launched pulse. This delay is proportional to the distance from the source. Typical output of an O.T.D.R display is shown in Figure 2 for reflections and backscatter [6]. More information can be found in references 4 and 5.

The advantages of using this technique for Optical Fiber Sensors is that measurements can be taken along a long fiber length with many sensors in series and that losses can be analyzed locally.

1.1.4 OPTICAL FREQUENCY DOMAIN REFLECTOMETER

By applying a frequency modulation to the optical source at the detector, and then converting the propagation delay into a beat frequency, the O.F.D.R is a similar technique for measurements of local losses. The advantage of this method over the O.T.D.R is higher accuracy and better time response [5].

1.1.5 THE MICROBENDING EFFECT

A change in the refractive index due to bending was found to be one of the major reasons for losses in optical fibers [7]. Therefore, this change can be used to make strain/displacement sensors once the bending of the fiber is related to mechanical strain or displacement.

By bending an optical fiber at an optical resonance pitch, F1, the amount of power loss will increase exponentially at very small deflections, particularly in multimode fibers. The frequency pitch was found to be [8]:

$$F1=\frac{2\pi}{Kc} \qquad (1)$$

where Kc is a property of the refractive index difference and the fiber radius. For a fiber with a parabolic index profile

$$k_c = \frac{\sqrt{2\Delta}}{a} \tag{2}$$

where a is the fiber radius and Δ is the max relative index difference and is equal to:

$$\Delta = \frac{(n_1^2 - n_2^2)}{2n_1^2} \tag{3}$$

with n_1 and n_2 equal to the refractive index for the core and cladding respectively. The attenuation of a fiber with a parabolic index profile and curved axis was derived to be [8]:

$$F(l) = \{L^{-1/2} \int_{-L/2}^{L/2} f(z,l) \exp(-iK_o) dz\}^2 \tag{4}$$

The function, f(z,l), is the deviation from the straightness along the fiber axis z, and L is the total length of the curved fiber such that $-L/2 \leq z \leq L/2$. The sensitivity to deflection when the loading pitch is within the range of the microbending (optical) resonance was found to be extremely high for deflections which are two orders of magnitude less then the fiber diameter [9].

1.2 INTENSITY STRAIN AND DISPLACEMENT SENSORS REVIEW

Intensity modulation strain and displacement sensors have already been investigated and reported [1,2,4,5,11,12]. The principles of microbending and

Optical Time Domain Reflectometry were both used to prove the feasibility of strain and displacement fiber optic sensors. In one application a step index plastic fiber was heated and prefabricated with its mechanical wavelength of microbending [10]. A tension bar specimen was axially loaded and losses versus strain/displacement were taken. Typical losses in the order of 0.5V per 0.1mm' of displacement were achieved for gage length of 19mm'.

The bending of large structures has been measured by the use of a microbending sensor [11]. A flexible U shape frame was firmly attached to the structure. A lower portion of the microbender mechanism was part of this frame. A rigid rod was firmly attached to the upper part of the U profile, and included the upper part of the microbending mechanism. An optical fiber was placed between the two parts of the microbending mechanism in the length direction of the structure member. Bending in the structure caused deflection of the upper part of the microbending mechanism towards the lower part. A change of the transmitted light, due to the microbending effect, was measured by an optical detector. The power attenuation achieved 10 db for curvature of 2.7/kilometer. An O.T.D.R was used to detect losses from three different sensors which were about 50 meters apart.

The principle of fiber segmentation was used to measure fiber strain [12]. A sensing waveguide was physically segmented into discrete sections. By

monitoring the shifting of the near and far ends reflected pulses from an O.T.D.R of each individual segment, strain (and temperature), changes can be calculated. Those reflections were due the glass–air–glass interface provided by partially reflective splices. Improving the sensitivity of the time domain based strain (and temperature), the length of the sensing fiber was increased virtually by recirculating the probing pulse through the fiber with special tap–off couplers. Typical outputs of such a sensor achieved a delay of 100ps for 500μm of fiber elongation, with N=50 cycles of fiber recirculations.

A loss compensation of intensity modulation fiber optic sensor was used for displacement measurement [13]. Light enters two fiber optics coupled to one fiber. The light is transmitted to a mirror image of the source side through air gap. Lateral displacement changes the transmitted/reflected ratio. Reading of reflectance and transmission level from the four ends of the sensor enables compensating the losses from the connections and the fiber lines. This sensor was found sensitive to displacements from 10 to 80 μm. The standard deviation of fixed displacement and 50 disconnecting/connecting cycles was 0.11 percent of full scale.

Many other sensors for strain and displacement are also reported in the literature however, the number of sensors available today for industry use is very small, if any.

1.3 THE ORIENTATION ANGLE APPROACH

The behavior of glass and other fibrous materials crossing a crack in fiber reinforced concrete and other composite materials has been investigated [15–19]. In reference 15, the elastic deformation of a metal fiber crossing a crack at some orientation angle, was analyzed using elementary beam theory. The force created by the matrix reaction on the fiber was approximated as a uniform stress acting along a certain length of fiber embedded inside the matrix.

Another approach to analyzing stresses in a fiber crossing a crack was presented in reference 16. Glass fiber reinforced cement composites were evaluated for the effect of orientation angle using simple beam bending theory and assuming that the uniaxial tensile stress on the fiber is small compared to the bending stresses. Bending stresses were approximated by geometric relations of the crack and the fiber diameter and radius of curvature. For the simple beam bending theory, the length of the fiber inside the matrix in which reaction forces are acting is unknown and must be approximated. For the purpose of crack detection it is necessary to use matrix materials which have pure elastic behavior. This will ensure that both the fiber (glass) and the matrix will maintain their elastic properties after a failure in the matrix. The deformation of the matrix in the reaction to the bending of the fiber after crack initiation is pure elastic and can be expected to be reproducible in cycling loading.

In the current work reported here, the use of pure elastic materials for both the fiber and matrix allows the use of the theory of beams on an elastic foundation to investigate the elastic curve of an optical fiber crossing a crack. In addition, the fact that the elastic curve changes signs when this theory is used will provide a better input for the calculation of the power attenuation which is very sensitive to changes in curvature. The lack of information on the length of the fiber inside the matrix over which forces are acting can be solved by using a partially supported semi-infinite beam model where the actual length is evaluated at the point where the deflection is approximately zero.

1.3.1 GEOMETRIC MODEL

Figure 3 illustrates a fiber optic crossing a crack. It can be seen that when the fiber creates an orientation angle (Θ) with the crack less than 90^0, the fiber bends at both boundaries of the crack. Bending in the fiber is symmetric with the point of symmetry at O in Figure 4. A more general case can be analyzed by assuming initial conditions of fiber crossing an initial air gap with additional crack opening displacement (cod). The benefit of studying this case is that strains are reduced from infinity when a crack initially appears.

In Figure 4, L0 is one half of the initial air gap ($\delta/2$ in Figure 3) and L1 is the

additional displacement in the matrix due to the crack opening displacement. The-X axis is along the direction of the original fiber orientation, Θ, and the Y-axis is in the direction of bending. Point B in Figure 4 changes place horizontally to point B', but is deflected vertically as a result of the elastic foundation spring constant. The following geometric relations can be evaluated.

Total deflection of the fiber relative to point O, Y0, is

$$y0=\frac{L1}{\sin\theta} \tag{5}$$

where the actual length of the two sections of fiber crossing the air gap after additional displacement, L1, in the direction of X are respectively:

$$S0=\frac{L0}{\cos\theta} \tag{6}$$

$$S1=L1\cos\theta \tag{7}$$

This geometric model divides the problem of analyzing deflections in a fiber optic crossing a crack into two regions. Region 1 was analyzed as a cantilever beam and includes the initial gap, L0, and the additional displacement L1. Region 2 was analyzed as a semi-infinite beam on a elastic foundation and starts at the boundary between the air gap and the matrix at point B' and theoretically ends at infinity where no deflection exists.

1.3.2 THE THEORETICAL MODEL FOR DEFLECTIONS

As presented in section 1.3.1, a fiber optic crossing a crack, can be modelled as a beam which has two regions as shown in figure 5. Region 1 is a cantilever beam subjected to a vertical force P at the symmetry point, O, and has an initial slope $y'_{2(x2=0)}$ and deflection $y_{2(x2=0)}$ input from Region 2 of the elastic foundation as shown in figure 6.

The actual fiber length, L, in the direction of the orientation angle, Θ, includes an additional displacement of the crack opening displacement, L1. The sum of these two parts is L=S0+S1 (Figure 4), and equals:

$$L=\frac{L0+L1COS^2\theta}{COS\theta} \qquad (8)$$

The elastic curve or deflected shape of the fiber passing through the two regions is shown in Figure 6. The deflection at point of symmetry, O, is geometrically constrained to Y0. At the boundary between the two regions (point B'), continuity in deflection, y, and slope, y', is maintained.

Two problems must be solved.

1. A Cantilever beam with a force, P, at the free left end and an initial slope, $y'_{2(x2=0),}$ and deflection, $y_{2(x2=0),}$ at the fixed right end.

2. A semi-infinite beam on an elastic foundation with force, P, and moment, M_l, at the left end.

For problem 1, the origin of the axis system is assumed at the left end of the beam and from elementary beam theory the differential equation

$$E_f I_f y'' - Px = 0 \tag{9}$$

where E_f is the material modulus of elasticity, I_f is the beam moment of inertia, and $y''=d^2y/dx^2$

is used which assumes no axial load. The conditions for this assumption are discussed in the next chapter.

After integration and applying boundary conditions for zero deflection and slope at x=L, the expressions for slope and deflection are:

$$y' = +\frac{px^2}{2E_f I_f} - \frac{pL^2}{2E_f I_f} \tag{10}$$

$$y = \frac{P}{6E_f I_f}(2L^3 - 3L^2 x + x^3) \tag{11}$$

Including the boundary conditions for slope and deflection at the right end of the beam, and accumulating deflections along the beam, the deflection at any point X on the cantilever beam is expressed as

$$y(x)=y_{2(x2=0)}-y'_{(x2=0)}(L-x)+\frac{p}{6E_fI_f}(2L^3-3L^2x+x^3) \quad (12)$$

Substituting the deflection, Y0, at the origin (x=0) into Equation 12 yields:

$$Y0=y_{2(x2=0)}-y'_{2(x2=0)}L+\frac{pL^3}{3E_fI_f} \quad (13)$$

With P known, the initial slope and deflection can be defined.

For the solution of problem 2, the Winkler theory of beams on an elastic foundation [18] is used. The governing fourth order equation for the general case of moments, axial force,N, and elastic foundation spring force is:

$$E_fI_f\frac{d^4y}{dx^4}-N\frac{d^2y}{dx^2}+K_sy=0 \quad (14)$$

where K_s is the elastic foundation constant.

Substituting $y=e^{mx}$, the characteristic equation becomes:

$$EIm^4-Nm^2+K_s=0 \quad (15)$$

and the four roots for m are:

$$m_{1,2,3,4}=\pm\sqrt{\frac{N}{2E_fI_f}\pm i\sqrt{\frac{K_s}{E_fI_f}-(\frac{N}{2E_fI_f})^2}} \quad (16)$$

yielding a general solution of:

$$y=A_1e^{m_1x}+A_2e^{m_2x}+A_3e^{m_3x}+A_4e^{m_4x} \tag{17}$$

The relationship between N and $2\sqrt{(E_fI_fK_s)}$ which come from the small root affect the final solution.

For the case of $N<2\sqrt{(E_fI_fK_s)}$, which exists for the optical fiber and matrix in use and will be discussed in the next chapter, the solution of Equation 17 is:

$$y_2=(c_1e^{\alpha x}+c_2e^{-\alpha x})\cos(\beta x)+(c_3e^{\alpha x}+c_4e^{-\alpha x})\sin(\beta x) \tag{18}$$

where

$$\alpha=\sqrt{\sqrt{\frac{K_s}{E_fI_f}}+\frac{N}{4E_fI_f}} \tag{19}$$

and

$$\beta=\sqrt{\sqrt{\frac{K_s}{4E_fI_f}}-\frac{N}{4E_fI_f}} \tag{20}$$

The case of a semi-infinite beam requires that when x goes to infinity the deflection and moment approach zero which causes c_2 and c_4 in Equation 18 to

equal zero.

The solution of Equation 18 when moment, M_l, and force, P, are applied to the beam is done by superposition of the two load cases shown in Figure 7.

The equations for deflection, slope and moment for case 1 (force) and case 2 (moment) are developed by applying free end boundary conditions at $x_2=0$ [18] and are as follows:

$$y_{21}=\frac{P}{\beta K_s}2\frac{\lambda^2}{(3\alpha^2-\beta^2)}e^{-\alpha x}[2\alpha\beta\cos(\beta x)+(\alpha^2-\beta^2)\sin(\beta x)] \tag{21}$$

$$y'_{21}=-\frac{P}{EI_f}\frac{1}{3\alpha^2-\beta^2}\frac{1}{\beta}e^{-\alpha x}[\beta\cos(\beta x)+\alpha\sin(\beta x)] \tag{22}$$

$$M_{21}=-\frac{P}{\beta}2\frac{\lambda^2}{3\alpha^2-\beta^2}e^{-\alpha x}\sin(\beta x) \tag{23}$$

$$y_{22}=\frac{M_l}{EI_f}\frac{1}{3\alpha^2-\beta^2}\frac{e^{-\alpha x}}{\beta}[\beta\cos(\beta x)-\alpha\sin(\alpha x)] \tag{24}$$

$$y'_{22}=-\frac{M_l}{EI_f}\frac{1}{3\alpha^2-\beta^2}\frac{1}{\beta}e^{-\alpha x}[2\alpha\beta\cos(\beta x)-(\alpha^2-\beta^2)\sin(\beta x)] \tag{25}$$

$$M_{22}=-M_I\frac{1}{3\alpha^2-\beta^2}\frac{1}{\beta}e^{-\alpha x}[(3\alpha^2-\beta^2)\beta\cos(\beta x)-(\alpha^2-3\beta^2)\alpha\sin(\beta x)] \quad (26)$$

Combining results from the load conditions and simplifying, yields the solutions for a semi-infinite beam on elastic foundation.

$$y_2=y_{21}+y_{22}=\frac{e^{-\alpha x}}{Q\beta}\{[2\alpha\beta\cos(\beta x)+(\alpha^2-\beta^2)\sin(\beta x)]\frac{P}{K_s}2\lambda^2+\frac{M_I}{E_fI_f}[(\beta\cos(\beta x)-\alpha\sin(\beta x))]\} \quad (27)$$

where $Q= 3\ \alpha^2 - \beta^2$

$$y_2'=-\frac{e^{-\alpha x}}{E_fI_fQ\beta}\{M_I[2\alpha\beta\cos(\beta x)-(\alpha^2-\beta^2)\sin(\beta x)]+P[\beta\cos(\beta x)+\alpha\sin(\beta x)]\} \quad (28)$$

$$M_2=-\frac{e^{-\alpha x}}{\beta Q}\{M_I[Q\beta\cos(\beta x)-(\alpha^2-3\beta^2)\alpha\sin(\beta x)]+2P\lambda^2\sin(\beta x)\} \quad (29)$$

The boundary conditions at point B' (Figure 5) are found by substituting $X_2=0$ into Equations 27 and 28.

$$y_{2(x_2=0)}=\frac{1}{Q}(\frac{4P\lambda^2\alpha}{K_s}-\frac{M_I}{E_fI_f}) \quad (30)$$

$$y'_{2(x2=0)} = -\frac{1}{E_f I_f Q}\{M2\alpha - P\} \tag{31}$$

These results are substituted into Equation (13) and the solution for deflection in case 1 (cantilever beam) is simplified as

$$y(X) = \frac{1}{Q}\{4P\lambda^2\frac{\alpha}{K_s} + \frac{M_1}{E_f I_f}\} - \frac{1}{E_f I_f Q}\{M2\alpha + P\}(L-X) + P\frac{(2L^3 - 3L^2X + X^3)}{6E_f I_f} \tag{32}$$

At the point of symmetry, O, X=0 and Equation 32 becomes:

$$Y0 = y_{2(x2=0)} - y'_{2(x2=0)}L + \frac{PL^3}{3E_f I_f} \tag{33}$$

from which P is equal to

$$P = \frac{Y0}{K_1} \tag{34}$$

and K_1 is equal to

$$K_1 = 4\lambda^2\frac{\alpha}{QK_s} + \frac{L}{QE_f I_f} - 2\alpha\frac{L^2}{E_f I_f Q} - \frac{L}{E_f I_f Q} + \frac{L^3}{3E_f I_f} \tag{35}$$

For the interesting case when $N << 2\sqrt{(K_s E_f I_f)}$

$$\alpha = \beta = \lambda = \sqrt[4]{\frac{K_s}{E_f I_f}} \tag{36}$$

The solutions for deflection, slope, and moment for case 2 reduce to:

$$y2(x_2)=e^{(-\lambda x)}\ \{\ [2P\frac{\lambda}{K_s}\cos(\lambda x)+\frac{M_1}{2E_fI_f\lambda^2}[\cos(\lambda x)-\sin(\lambda x)]\ \} \tag{37}$$

$$y'_2(x_2)=-e^{(-\lambda x)}\ \{\ \frac{P}{2E_fI_f\lambda^2}\cos(\lambda x)+\frac{M_1}{E_fI_f\lambda}(\cos(\lambda x)-\sin(\lambda x)\ \} \tag{38}$$

$$M_2(x)=e^{(-\lambda x)}\ \{\ M[\cos(\lambda x)-\sin(\lambda x)]-\frac{P}{\lambda}\sin(\lambda x)\ \} \tag{39}$$

Substituting X_2=0 into Equation 32 which reduced to

$$Y0=Y_{2(x2=0)}-y'_{2(x2=0)}+\frac{PL^3}{3E_fI_f}$$

The load, P_2, for this case is

$$P_2=\frac{Y0}{K_2} \tag{41}$$

and

$$K_2=2\frac{\lambda}{K_s}+\frac{L^2}{E_fI_f\lambda}+\frac{L}{E_fI_f\lambda^2}+\frac{L^3}{3E_fI_f} \tag{42}$$

1.3.3 THEORETICAL RESULTS

Equations for deflection, slope, and moment, along a partially-supported semi-infinite beam on an elastic foundation were developed in Section 1.3.2. The solution of these equations requires a value for the force P. Equations 34 and 41 provide solutions for P for cases with and without an axial force, N, respectively. These equations are dependent upon the orientation angle, Θ, initial half gap opening, L0, additional half crack opening displacement, L1, fiber (beam) properties, $E_f I_f$, and the elastic foundation constant Ks. The inequality

$$N<2\ E_f I_f Ks$$

required for equation (18) was verified using the following fiber optic material properties:

E_f= 10.6E+06 psi.

D_f=0.00492 inch (0.125 millimeter).

$I_f=\pi/64*D_f^4$.

Ks=250 ksi, 500 ksi, 750 ksi.

Selection of the actual elastic foundation constant, Ks=500 ksi, was based on test results of the epoxy in use. Using the inequality for the axial force, N, values of 17.46 lbs and 30.35 lbs were calculated for elastic foundation constants of 250 ksi and 750 ksi respectively. The tensile strength of a piece of bulk glass is approximately 700 ksi. However, the presence of stress concentrating microscopic flaws will reduce the effective strength to 100 ksi – 200 ksi [20]. Probability of

fiber failure is 0.01 when stress is in this range and increases exponentially when stresses are 300 ksi or greater. A typical proof stress test requirement for communication fiber (as used in our tests) is 50 ksi. The resultant tensile force, F_t, that the fiber in use can hold for tensile stress of 200 ksi is 4 lb. This value is much smaller than the inequality for N with elastic foundation constant of 750 ksi, and verifies the use of Equations 19 and 20 and the solutions defined in Equations 32 to 35.

Fiber bending occurs when the orientation angle, Θ, is greater than zero. This angle reduces the actual axial force in the fiber by $\cos(\Theta)$. For small values of additional crack opening displacement, L1, with respect to the initial gap opening, L0, the axial force will not reach the fiber breaking load. In cases where $N<<F_t$, the inequality for N becomes $N<<2\sqrt{E_f I_f K_s}$ and Equations 36 to 42 for deflection, slope and moments are effective. The assumption of $N<<F_t$ is verified in testing if no failures occur in the fiber for small values of orientation angle, Θ.

Each of the cases of deflection of fiber optic crossing a crack shown in Figures 8, 9, and 10, was solved for force P with respect to the orientation angle, Θ, and the initial gap opening, L0. The additional half crack opening displacement, L1, was 0.001" (20% strain) in all cases. The results for deflection, Y, along the fiber axis, X, are plotted for the following cases.

Figure 8 shows 3 separate deflection curves for initial gap openings of 0.005", 0.01" and 0.015". The orientation angle was $\Theta=30^0$, and the elastic foundation constant was 500 ksi for all three curves in this figure. From the figure, it can be seen that as L0 decreases, deflection and curvature will increase. Similar behavior occurs for decreases in orientation angle, Θ. The smaller the angle, the smaller the deflection and curvature in the beam.

Three deflection curves are shown in Figure 9 for orientation angles of $\Theta=15^0$, 30^0, and 45^0. The initial gap opening, L0, was 0.005" and the elastic foundation constant was 500 ksi.

Another three deflection curves are shown in Figure 10 for elastic foundation constants of K_s=250 ksi, 500 ksi, and 750 ksi. The initial gap opening, L0, was 0.005", and the orientation angle, Θ, was equal to 30^0. As expected, an increase in the elastic foundation constant results in an increase of the total deflection (and curvature).

The equation for the bending stress in the fiber is $\sigma_b=M(x)*(D_f/2)/I_f$ where $D_f/2$ is the fiber radius, M(x) is the bending moment as defined for each case and I_f is the fiber moment of inertia. Bending stresses in the fiber for elastic foundation constant of 250 ksi, 500 ksi, and 750 ksi are plotted in Figure 11 and cases for Ks=500 ksi and Θ= 15°, 30°, 45° were plotted in Figures 12, 13 and 14. The

orientation angle used was 30^0, which represents an average value used for testing, and the initial gap opening was 0.005", which produces the worst case. From the graphs, it can be seen that changes in elastic foundation constant and in orientation angle, Θ, have a significant influence on bending stresses. The maximum stress was located at the elastic foundation region adjacent to the boundary of the cantilever beam and elastic foundation beam.

2. EXPERIMENTAL PROGRAM

The objective of the test program was to measure the power attenuation and to detect failure of a fiber optic crossing a crack as a function of orientation angle, Θ, and initial gap, L0. Two series of tests were established for this purpose. Test Type A (Figures 15 and 16), was conducted on a fiber optic embedded in a brittle adhesive matrix which was subjected to tensile forces from the top of a beam specimen. After a failure and initiation of a crack in the matrix, and as a result of the orientation angle, Θ, bending stresses are applied to the fiber. This results in power attenuation. Test Type B was conducted on an optical fiber crossing a crack, subjected to pure bending where no adhesive is needed and the elastic matrix is prefabricated (Figure 17). This test eliminates the effects of adhesive matrix curing on the output sensitivity.

Figure 15 illustrates the experimental setup block diagram for Test A. An Optical Time Domain Reflectometer was connected to a fiber optic cable which has a minimum length of 50 meters. This length of cable is necessary to get far enough away from the power source in order to let the input signal become stable from ringing and other effects. The fiber optic cable was connected through a splice or connector to a bare fiber. This fiber was embedded on the specimen over an initial gap (2*L0) by brittle adhesive matrix (epoxy) with orientation angle, Θ. The specimen, shown in Figure 16, was a cantilever beam subjected to a vertical force,

P, at the free end. From loading, the opening of the gap (2*L0) increased and the matrix was subjected to tensile strain. At some level of strain the matrix failed by cracking and produced bending in the fiber.

During the test the following parameters were measured:

* Crack opening displacement across the initial gap, was measured with a dial gage.

* Power attenuation was measured by the Optical Time Domain Reflectometer before and after cracking.

* Failure of the matrix was observed using a polarized filter which shows the photoelastic fringes produced from stress concentrations in the epoxy matrix over the initial gap. This technique is possible because the epoxy is photoelastic and behaves like a birefringent coating.

* Failure of the optical fiber was observed using the Optical Time Domain Reflectometer Display.

Specimen Preparation: Specimen preparation included adjusting the initial gap opening by measuring with feeler gages. Final adjustment was made with a microscope scale. The aluminum specimen shown in Figure 16 was then sanded to ensure reflectance of light and was cleaned in the area of the bonded matrix. The fiber coating was dissolved with methylene Chloride and then wiped with

optical paper. The fiber was then applied to the specimen at the required orientation angle with a very light preload and was temporarily secured in place before applying the epoxy (M Bond type AE by Measurement Group, with type 10 resin 100:15 mixing ratio). Resin and curing agents of the epoxy were mixed at a 100:15 ratio and cured overnight at a temperature of $115^0F \pm 5^0F$. To prevent the epoxy from filling the initial crack opening, silicon rubber was used.

The embedded fiber specimen was connected to the O.T.D.R and inserted in the loading machine. Loads from 0 to 200 lb. were applied at a very slow rate, to allow the O.T.D.R to update the screen with new data for load intervals less than 0.5 lb. The number of samples per each updated display was 64. At each load step, displacement, 2*L1, and backscatter loss measurement were taken. The epoxy was observed through the polarized filter to establish its fracture and provide a comparison to increasing losses in the O.T.D.R.

Figure 17 illustrates the specimen for Test B. This test differs from Test A in the following ways:

No matrix was applied to the specimen. The fiber was attached to the specimen through slots placed at the required orientation angle and was held by a plexiglass clamp. A displacement controlled test was performed with the load applied in the direction of the crack tips. This method of loading applies bending to the fiber and eliminates possible variations in matrix properties due to the curing process. The

nylon coating of the fiber was not removed to avoid possible local damage to the fiber from the clamp's edges.

Test type B procedure:

Specimen preparation included adjusting the initial gap opening (2*L0) by measuring with feeler gages at each end of the specimen. The specimen was attached to a 3 degree of freedom micropositioner which can easily control movements in all directions. The fiber was placed inside a slot on both sides of the air gap in the specimen and was clamped in place. The specimen was then connected to the O.T.D.R and fine adjustments were made to the micropositioner until initial losses and backlash were minimized. Incremental displacement was then applied to the fiber with backscatter losses being measured by the O.T.D.R. Table 1 presents the variation in parameters studied in both Test A and Test B.

Table 1: List of Tests and Parameters for type A and B Procedures.

No.	Test Type	LO (in.)	Θ (°)
1	A	0.005	15
2	A	0.005	30
3	A	0.005	45
4	A	0.01	15
5	A	0.01	30
6	A	0.01	45
7	A	0.015	15
8	A	0.015	30
9	A	0.015	45
10	B	0.005	30
11	B	0.005	45
12	B	0.01	30
13	B	0.01	45
14	B	0.015	30
15	B	0.015	45
16	A	0.007	15 (failure test only)
17	A	0.007	30 (failure test only)
18	A	0.007	45 (failure test only)

3. EXPERIMENTAL RESULTS AND CONCLUSIONS

3.1 EXPERIMENTAL RESULTS

The experimental results for power attenuation versus additional crack opening (2*L1) are shown in Figures 18 through 29. Figures 18 through 23 display results for cantilever beam specimens of test group A. Figures 24 through 29 display results for the displacement specimen of test group B.

In Figures 18 to 20, power loss is plotted as a function of additional crack opening displacement for three different half-gap openings, L0, with orientation angles, Θ, of 15, 30, and 45 degrees.

Figure 18 illustrates power attenuation along the optical fiber for $\Theta=15^0$. The three curves are for L0 values of 0.005", 0.01", and 0.015". In each curve power attenuation is undetectable (dead zone) for additional crack opening less than 0.001 inch. The turning point on the graph, at which the level of power attenuation was detected was found to be in agreement with photoelastic observations. The

photoelastic fringes created over the initial gap during loading, disappeared at the instant of the matrix cracking. At the same time, a significant change in power attenuation was also observed on the O.T.D.R. display. Maximum loss was for L0=0.01" which also had the longest zone of undetectable power attenuation in the figure. Output sensitivity was 0.09 to 0.18 db/mil and the "crack detection loss", which is the change in losses measured at the instant of matrix cracking, was 0.03 db to 0.2 db.

Figure 19 shows similar curves for an orientation angle of 30^0 and the same half initial opening displacements of 0.005", 0.01", and 0.015". The maximum "dead zone" observed was 0.0015" for the case of L0=0.015". Output sensitivity was 0.18 to 0.75 db/mil and crack detection losses of 0.1 to 0.2 db were measured.

In Figure 20, the three cases illustrated are for orientation angle of 45^0. The length of the maximum "dead zone" was 0.0017" for the case of L0=0.005". The higher values were for L0=0.005" and 0.01" which had the bigger dead zones. Output sensitivity was 0.08 to 0.51 db/mil and crack detection losses of 0.05 to 0.8 db were measured. Higher crack detection losses and larger "dead zones" were observed when L0 equals 0.005 and 0.01 inch.

The data was replotted in Figures 21 to 23 to compare results with respect to the orientation angle, Θ.

In Figure 21, the initial half opening, L0, was 0.005". For an Orientation angle of 15^0, the "dead zone" was 0.0002", and the crack detection loss was 0.4 db. For an orientation angle of 30^0, the "dead zone" was 0.0006" and the crack detection loss was 0.1 db. In the curve for $\Theta=45^0$, a very low level, but detectible zone was observed. At the end of this low level zone, a very clear crack detection loss of 0.5 db was observed. The average attenuation in the fiber was the highest for 45^0, and the lowest for 15^0 orientation angle after the observed dead zone.

The results plotted in Figure 22 are for an initial half-gap opening of 0.01". The maximum average attenuation loss was for the case of $\Theta=30^0$. Along the major of the range the attenuation for 45^0 was greater than those for 30^0. The lowest average losses occurred for 15^0.

Similar curves for initial half gap opening are shown in Figure 23. For this presentation of the data, the maximum average loss was for $\Theta=30^0$, and the

minimum was for $\Theta=45^0$.

Results shown in Figures 24 and 25 are for the test group type B, the displacement specimen, for initial half gap opening of 0.005", 0.01" and 0.015".

Figure 24 presents the power attenuation as was measured for orientation angle of 30^0 and 45^0 while the initial half gap opening is 0.005". The separation of the two curves from the origin is clear. An average loss of 0.6 db/mil was observed for 45^0, and 0.53 db/mil for 30^0.

In Figure 25, where the initial half gap opening was 0.01", average losses of 0.3 db/mil and 0.43 db/mil were observed for orientation angles of 30^0 and 45^0 respectively.

Figure 26 shows the attenuation along the fiber for initial gap opening of 0.015". Average losses of 0.2 db/mil and 0.23 db/mil are related to orientation angles of 30^0 and 45^0 respectively.

Presentation of the same data by holding the orientation angle in each figure and plotting the graphs for each initial half gap opening is shown in Figures 27 and 28. Figure 27 is for $\Theta=30^0$.

The data of the displacement specimen, test type B, was replotted in Figures 27 and 28, to compare the power attenuation results with variations of initial half gap openings.

As can be seen from Figure 27, the orientation angle was 30^0. The separation of the curves is clear over the deflection point of 0.004 inch. The power attenuation decreases when the initial gap opening is increased (lower strain), for the same orientation angle.

Figure 28 illustrates the results for orientation angle of 45^0. The separation of curves is clear from the very beginning. Here too, power attenuation decreases when the initial gap opening increases.

3.1.1 SUMMARY OF RESULTS

The experimental results obtained provide information with respect to crack detection limits, sensor output sensitivity for additional crack opening displacement, fiber optic failures and output behavior as a function of different geometrical parameters.

Crack detection levels were mostly for relative displacement (L1/L0) between 0.6%

to 6% of the initial gap opening displacement (L0) (eight of nine cases in test group A). The crack detection loss readout was mostly in the range of 0.1 to 0.5 db. The maximum loss for additional crack opening displacement of 0.006 inch in group A was from 0.45 db to 3.6 db. In six of the nine cases in group A, the output sensitivity was greater for those cases in which the dead zone was larger. For the same range of displacement in group B, loss power attenuation levels were from 1.25 db to 3.7 db. All tests of group A with initial half crack opening of 0.005 inch or more were successfully completed without fiber failure for an additional displacement of 0.006 inch. For an initial half gap opening of 0.0035 inch, failure in the fiber occurred for axial strains of 45% to 110%.

The power attenuation for different geometrical parameters in group A was not consistent for all tests. For tests with an initial half gap opening of 0.005 inch and 0.01 inch, the power attenuation increased for larger orientation angles. The case of L0 equal to 0.015 inch was different as the response for 45^0 was lower than 15^0 test. It is noted that this case had the smallest dead zone. The tests results for constant orientation angle and variations of initial gap opening showed unexpected behavior. For orientation angles of 15^0, and 30^0, the power attenuation increases while the initial gap opening increases (decreasing in strain). For an orientation angle of 45^0, the same test that was abnormal before (0.015 inch, 45^0), was also abnormal. This test showed losses less than the case of 0.005 inch.

The results of test type B showed that by increasing the strain, the power attenuation increased. For a fixed orientation angle power attenuation increases when the initial gap opening increases. For constant initial gap opening, power attenuation increases when orientation angle is increased.

A summary of the results is shown in Table No. 2.

Table 2 : Summary of Results for Tests Type A and B procedures

No. (Test type)	LO (inch)	Θ (degrees)	Detection Level (2L1) (inch)	Delection Loss (db)	Relative Displacement Detection level L1/ L0 (%)	Maximum Loss (db)	Fiber Failure Displacement Y/N (in.)
1(A)	0.005	15	0.0002	0.04	2	0.53	no
2(A)	0.005	30	0.0006	0.02	6	0.8	no
3(A)	0.005	45	0.0017	0.6	17	1.6	no
4(A)	0.01	15	0.0009	0.2	4.7	0.82	no
5(A)	0.01	30	0.0012	0.25	6	2.05	no
6(A)	0.01	45	0.0012	0.15	6	2.4	no
7(A)	0.015	15	0.0007	0.2	2.3	0.92	no
8(A)	0.015	30	0.0014	0.25	4.6	3.6	no
9(A)	0.015	45	0.0002	0.05	0.6	0.45	no
10(B)	0.005	30	-	-	-	3.2	no
11(B)	0.005	45	-	-	-	3.7	no
12(B)	0.01	30	-	-	-	1.9	no
13(B)	0.01	45	-	-	-	2.5	no
14(B)	0.015	30	-	-	-	1.25	no
15(B)	0.015	45	-	-	-	1.4	no
16(A)	0.0035	15	-	-	-	-	yes 0.0032
17(A)	0.0035	30	-	-	-	-	yes 0.0078
18(A)	0.0035	45	-	-	-	-	yes 0.0057

3.1.2 DISCUSSION OF RESULTS

The behavior of fiber optic crossing a crack was analyzed as a semi-infinite partially supported beam on an elastic foundation. A model for deflections and bending stress was developed. An experimental program was conducted to measure the power attenuation and to detect failures of such a fiber crossing a crack.

From the experimental and theoretical results we can learn about the phenomena that occur when a fiber is embedded in an elastic brittle matrix over an initial gap. The loading mechanism used and the air gap simulate crack initiation and propagation. Three major stages can be identified during the loading process. The first stage is the build-up of strain in the matrix over the air gap. The fiber is not bent, so almost no power attenuation can be detected. This stage ends when the matrix cracks. For the material used this happened mostly for strain level up to 6%. This number is in agreement with the matrix material properties for maximum elongation. The second stage starts when the matrix is cracked. A significant loss of power which appears at the time of cracking confirms that the fiber is subjected to bending stresses. Increasing of the loading also increases the power loss and ends at the fiber failure which defines the third and last stage.

The theoretical model for deflections and bending stress show a rise in stress when the orientation angle increases and the initial gap opening decreases. Both

behaviors were not verified by type A test result which appear to be quite random. The analytic model show high sensitivity of stress to the elastic foundation constant Ks. This property of the material is affected by the curing process of the matrix (epoxy) in use. Results from tests type A which are not consistent with the displacement specimen may be related to absorption of moisture by the matrix during curing and as a result to a change of elastic foundation constant. One solution to eliminate this problem during testing is the displacement specimen, type B, which does not use an on-site cured matrix and responded only to changes of geometric parameters. The results from tests type B suggest that the behavior of losses is similar to the theoretical behavior of bending stresses. Power attenuation is increases as the orientation angle increases and the initial gap opening decreases.

Failure in the fiber optic occurred only for initial half gap opening less than 0.005" which gave high strain levels. Analysis of bending stress shows that for axial strain level of 20%, the stress level is higher than 160000 psi for such a case. This is in agreement with the fact that fiber optic strength has low failure probability (0.01) for a stress level of 200000 psi and high probability over 300000 psi [20]. The axial strain level that was applied to the specimen show that failures in the fiber which was subjected to bending occurred for axial strains of 45% and higher, compared with 0.6 to 6 % of strain for the crack detection level. This gives the fiber enough reserve to be effective also for crack propagation measurements for initial half gap opening of 0.005" or more. The level of additional crack opening

displacement (2*L1), used in tests was 0.006" which is considered to be over practical applications for crack detection in mechanical and civil engineering.

3.2. CONCLUSIONS

A theoretical model for deflections and bending stresses in a fiber optic crossing a crack, was developed in Section 1.3.2. The model used assumed a partially supported semi-infinite beam on an elastic foundation. The model provided relations between the deflection of the fiber's neutral axis, the orientation angle of the fiber, Θ, and the initial gap opening ,2L0. The bending moments and stresses were evaluated for the same parameters. Calculations indicate that as orientation angle increases and initial gap decreases, the losses, which are related with stresses, should go up. Experimental work which was described in Section 2 and the results presented in Section 3.1 confirm the theoretical results. The control of the stresses in the fiber can be achieved by using materials with the appropriate mechanical properties for the elastic foundation constant and modulus of elasticity. A wide range of tests for orientation angles up to 45^0 and initial gap openings as low as 0.01" were undertaken without any failure in the fiber for displacement levels up to 0.006". The measured loss level for both detection of cracks and crack propagation were high in the order of 0.3db to 3.5db.

The current work suggests two kinds of fiber optic sensors. Both use the

orientation angle approach of a fiber optic crossing a crack. The proposed sensors provide more flexibility in attaching strain/displacement and crack detection sensors to structures as compared to available methods like strain gages. They have also the advantage of using fiber optic sensor technology which allows series connections for multi-sensor problems and immunity to environmental noise.

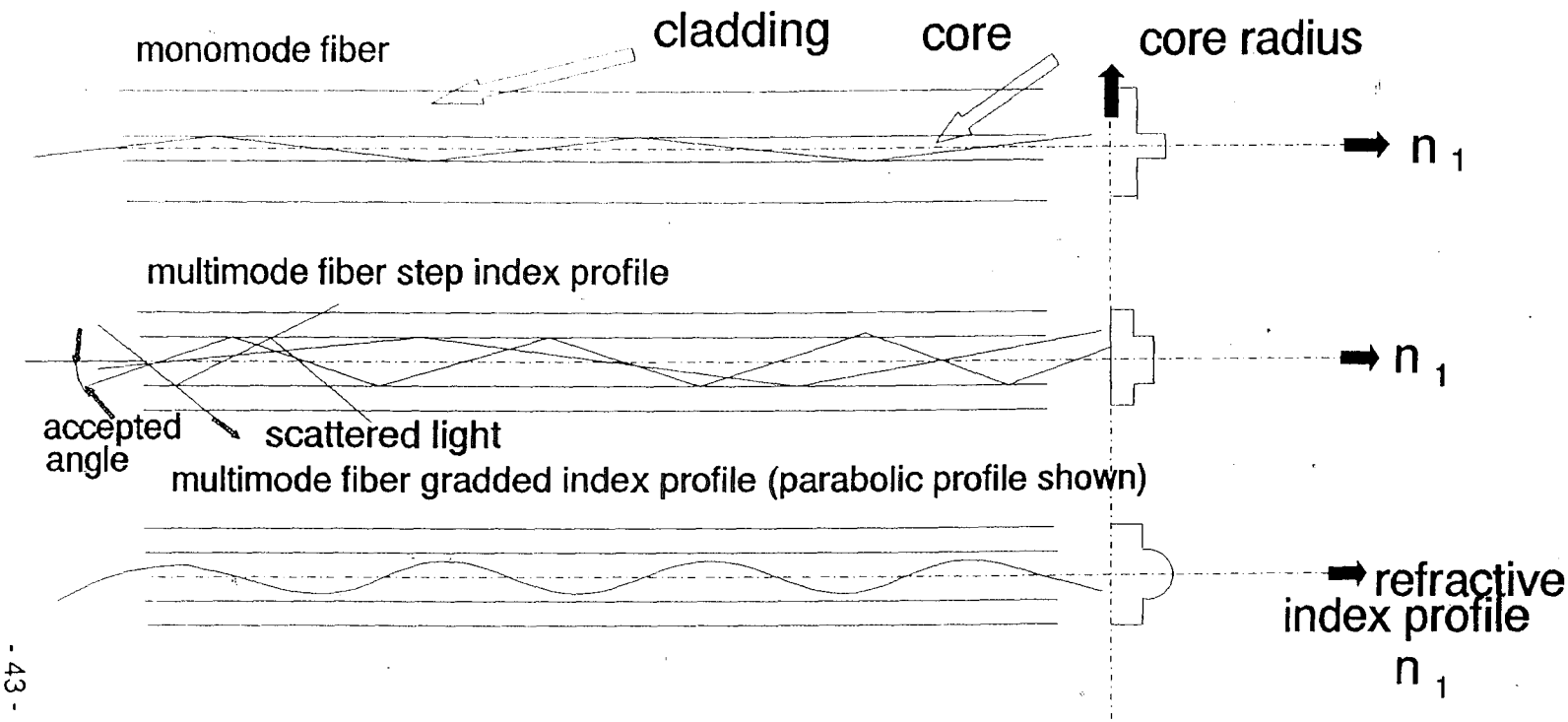

Fig.1- Monomode and Multimode Optical Fibers

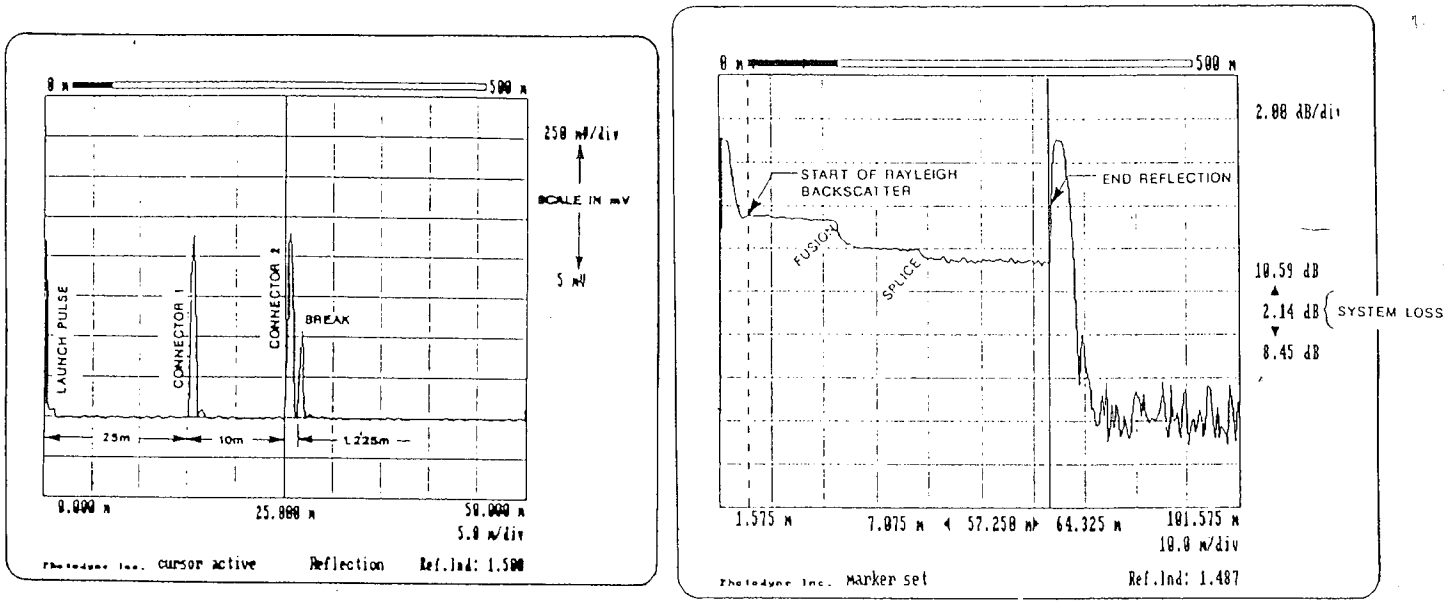

Fig. 2 - Typical O.T.D.R Outputs Display.

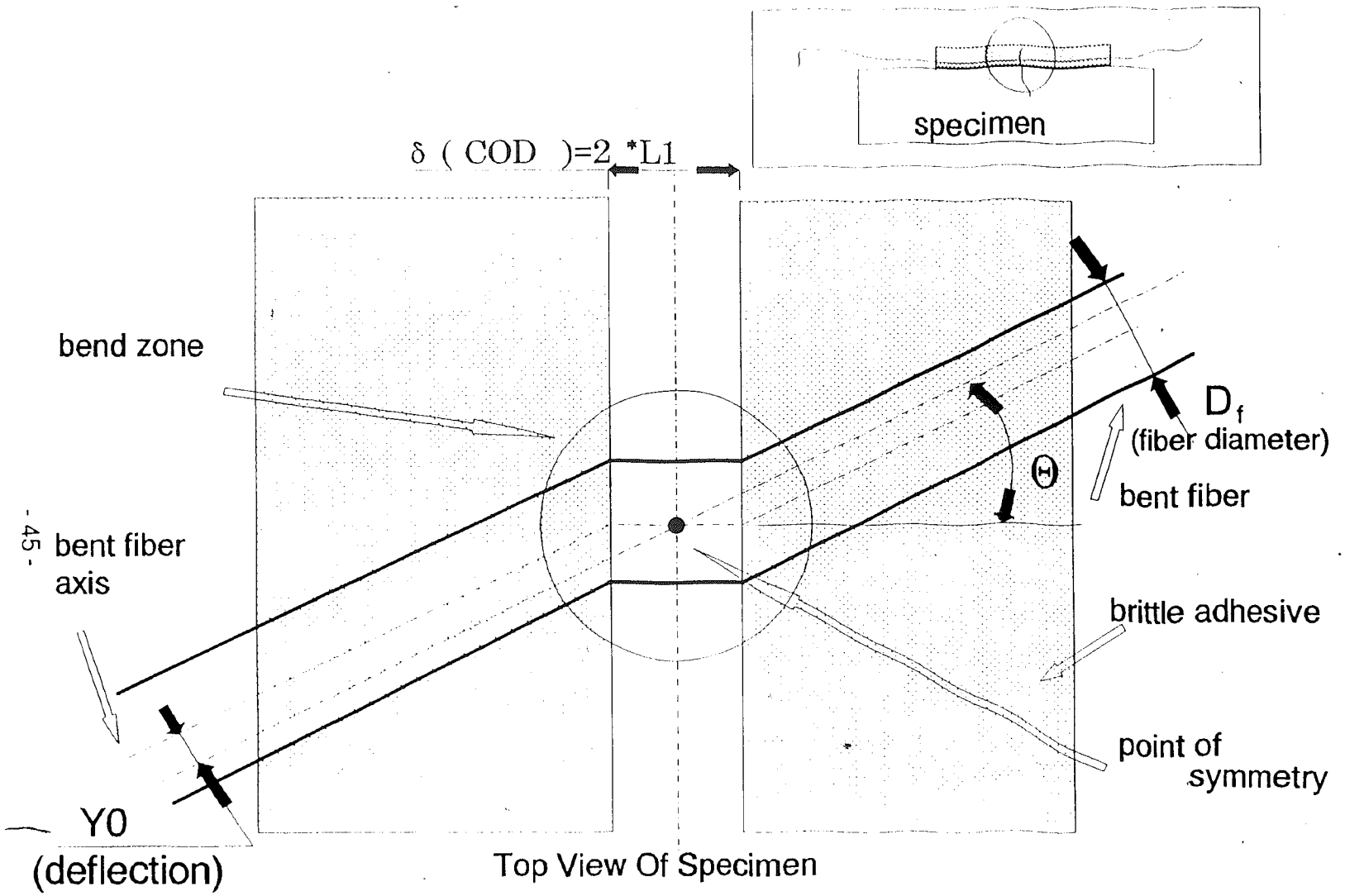

Fig. 3 - Fiber Optic Crossing a Crack.

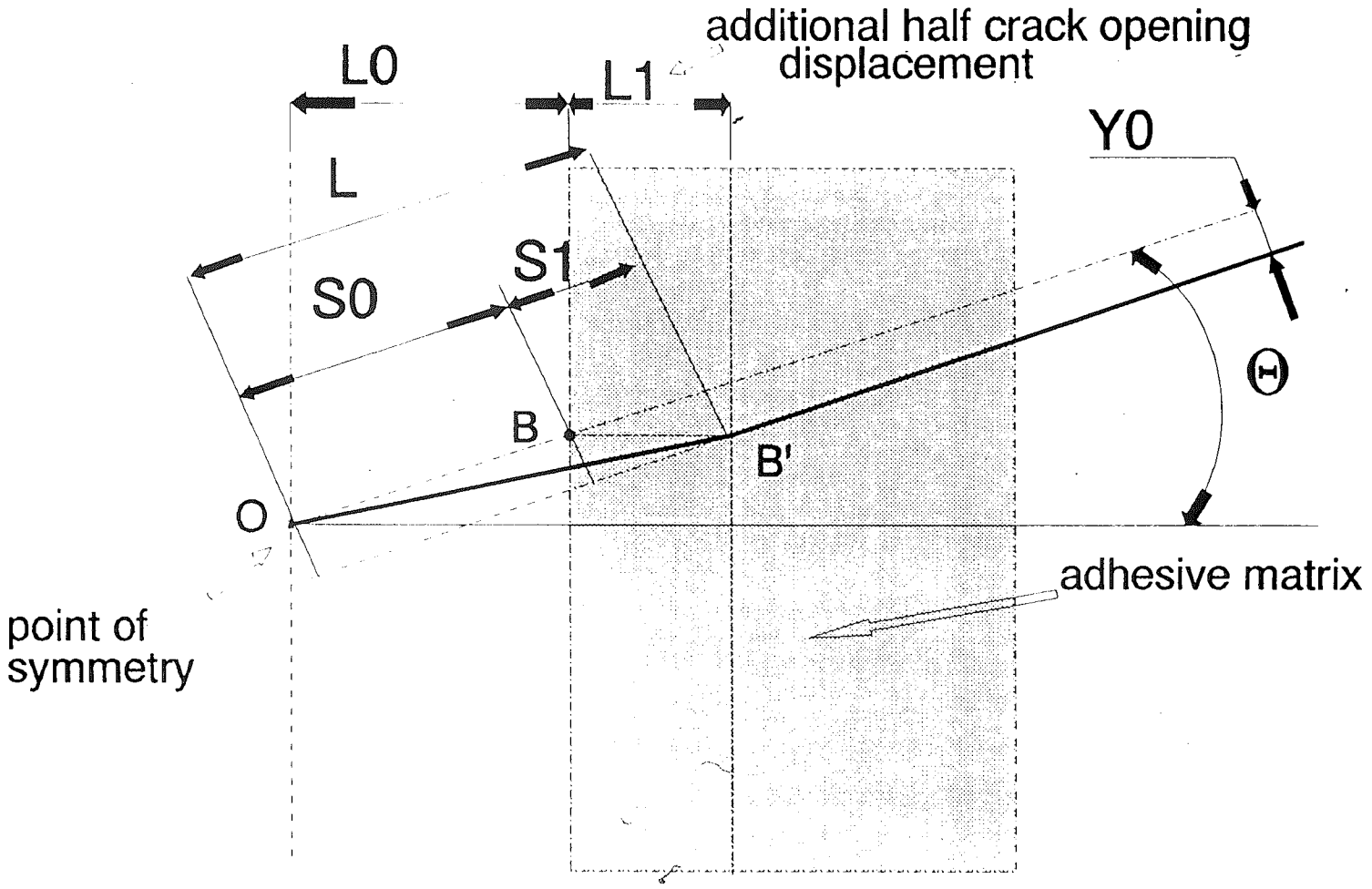

Fig. 4 - Geometric Model of Fiber Optic Crossing a Crack

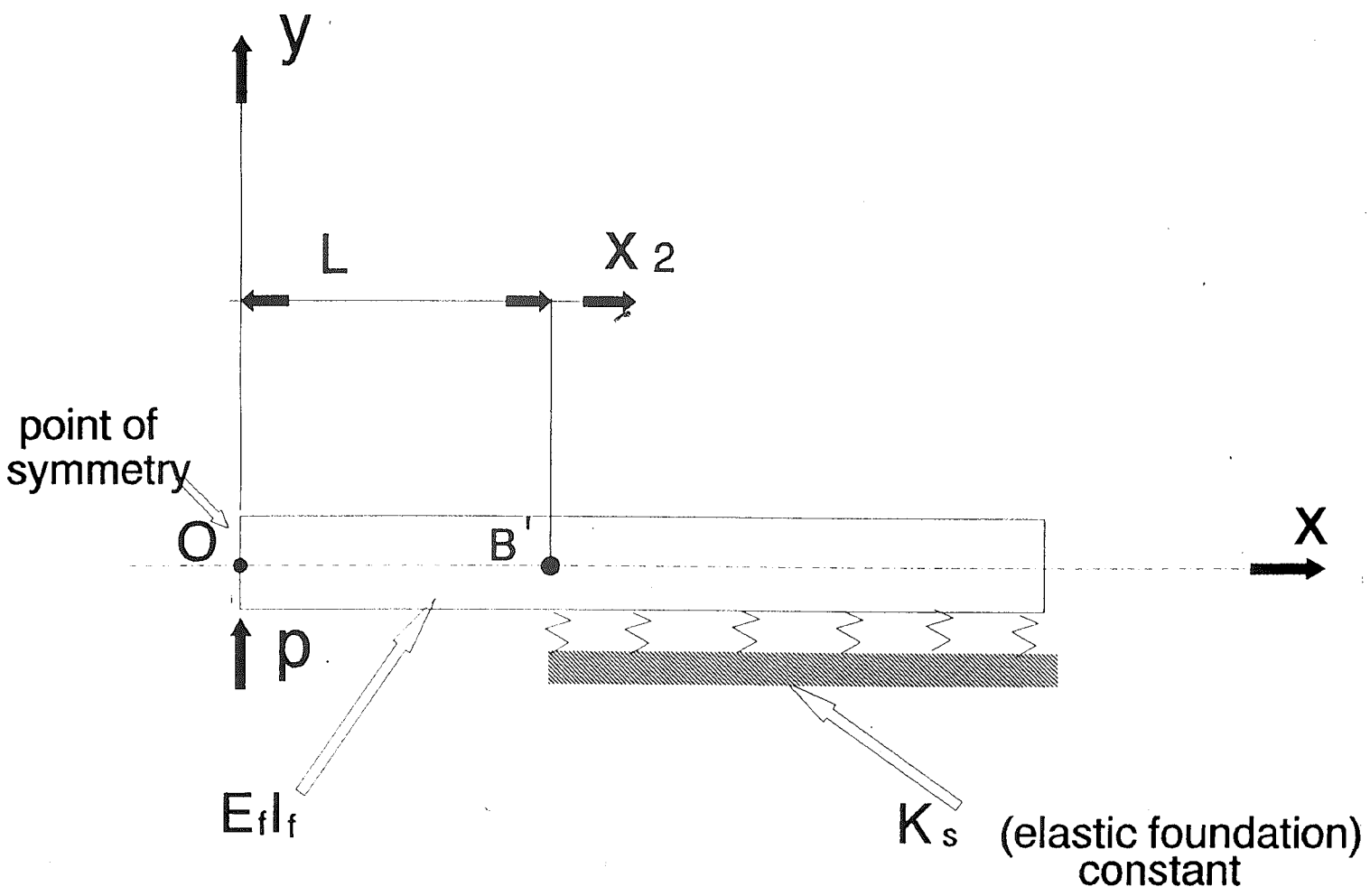

Fig. 5 - Semi infinite Partially Supported Beam Model

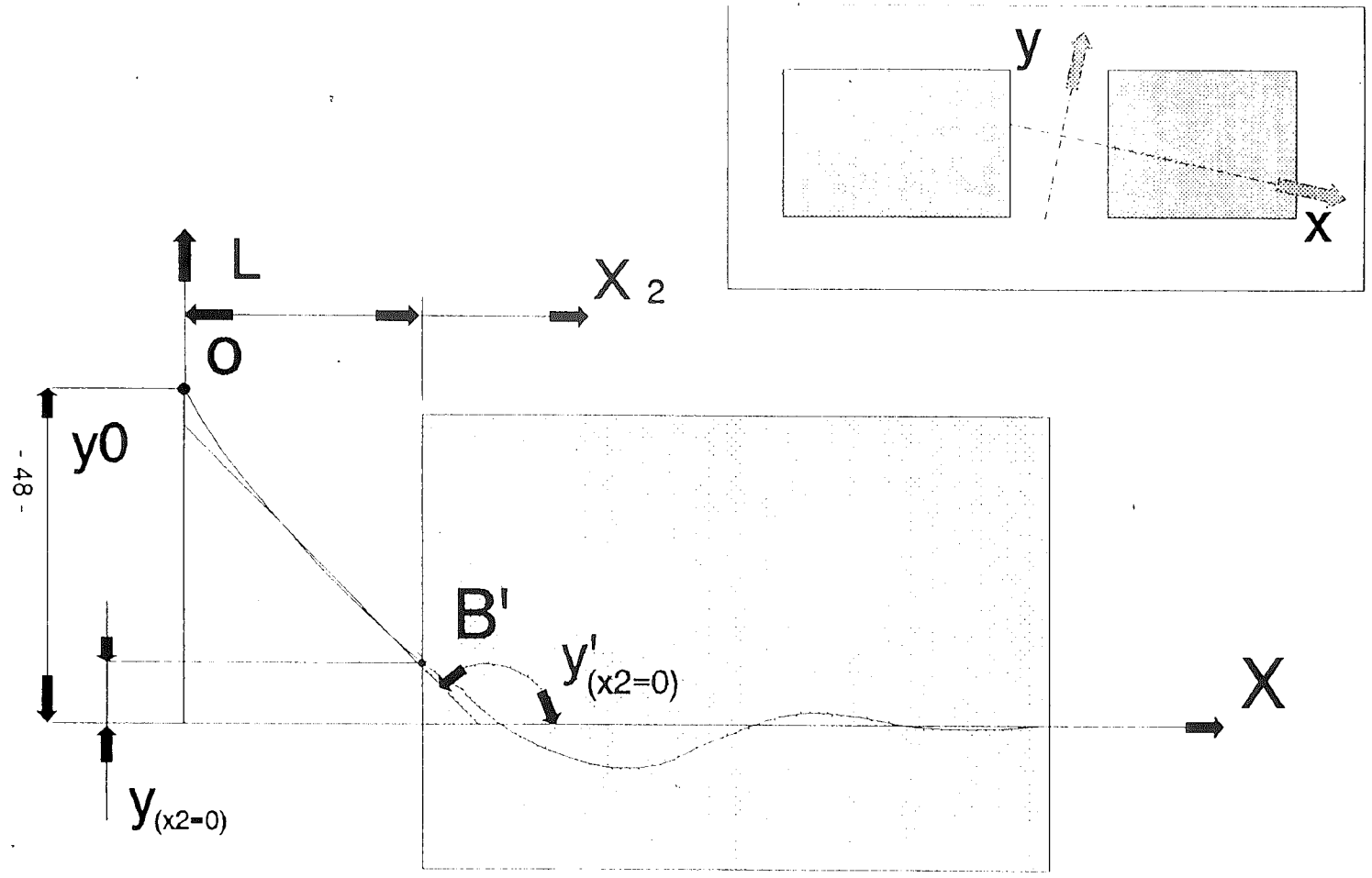

Fig. 6 Elastic Curve of Semi-Infinite Partially Supported Beam.

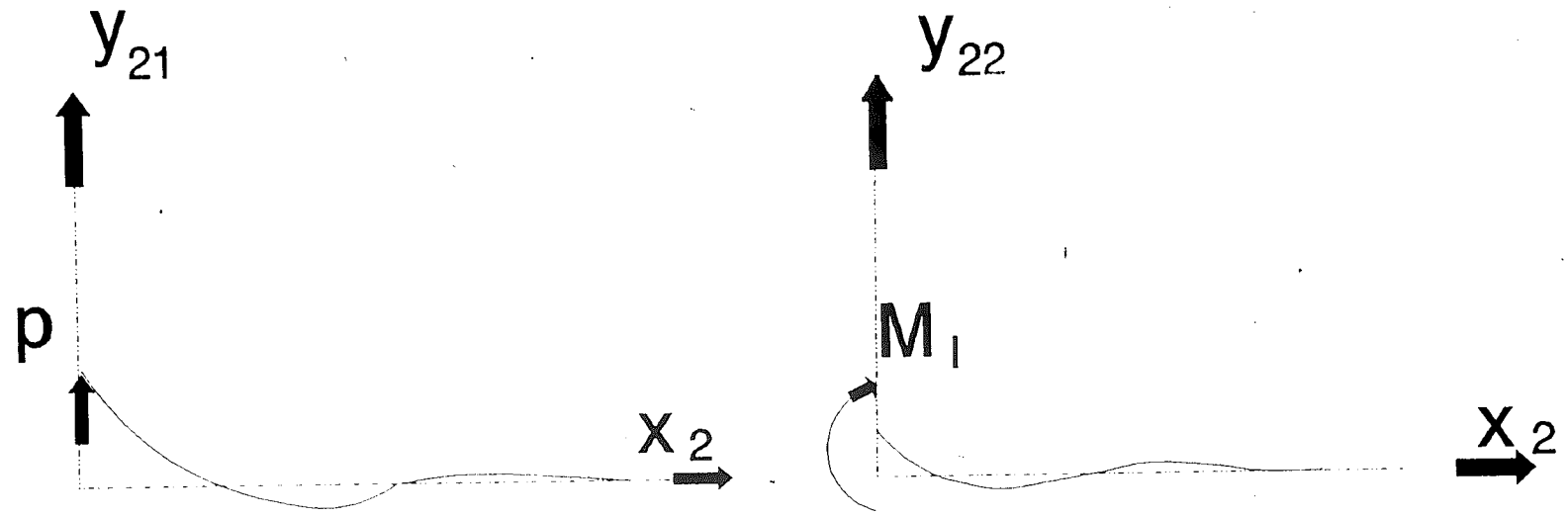

Fig. 7 Superposition of Force and Moment Cases of Beam in Elastic Foundation.

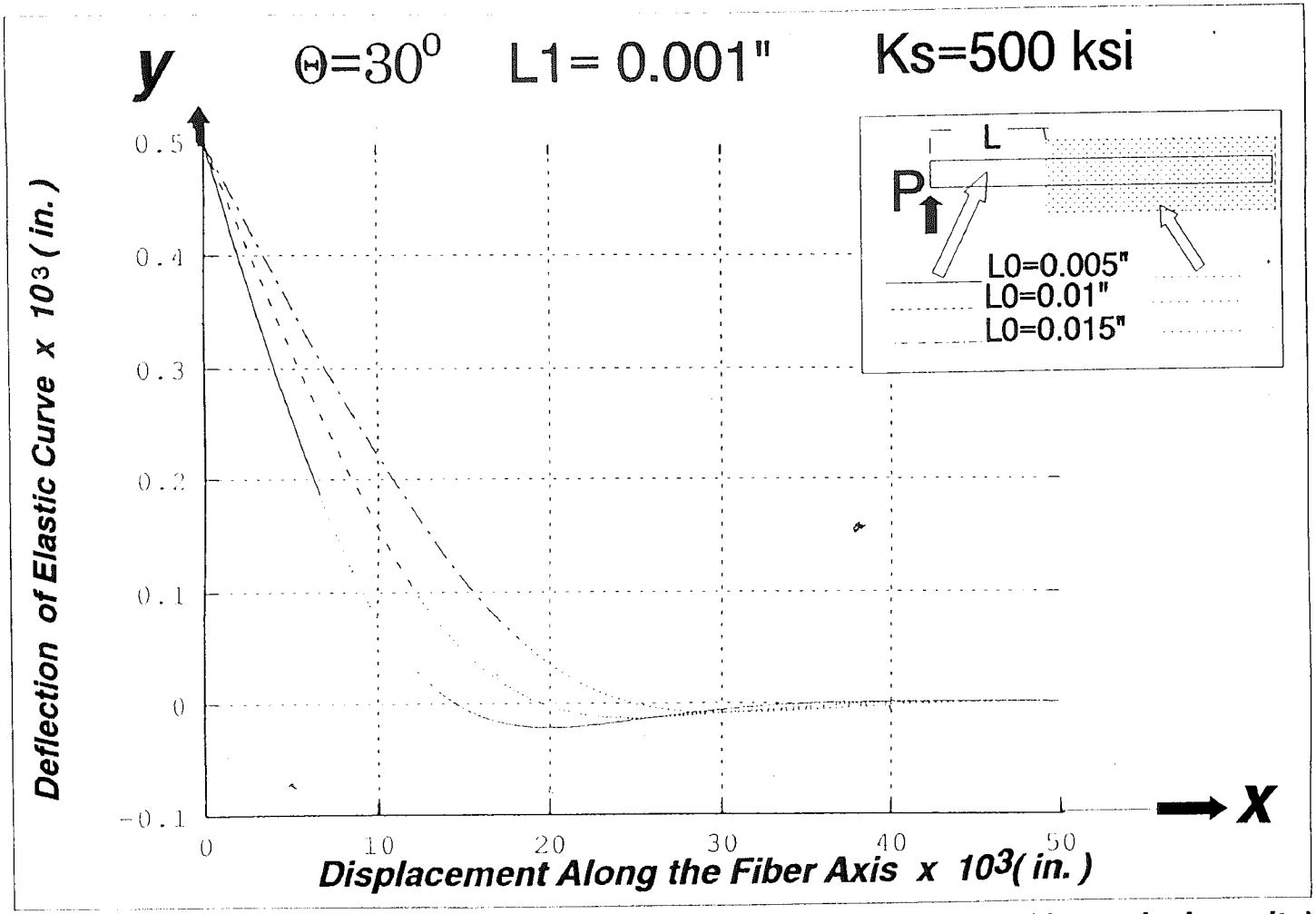

Fig. 8 - Variations of Elastic Curve with Changes in Initial gap L0 (theoretical results).

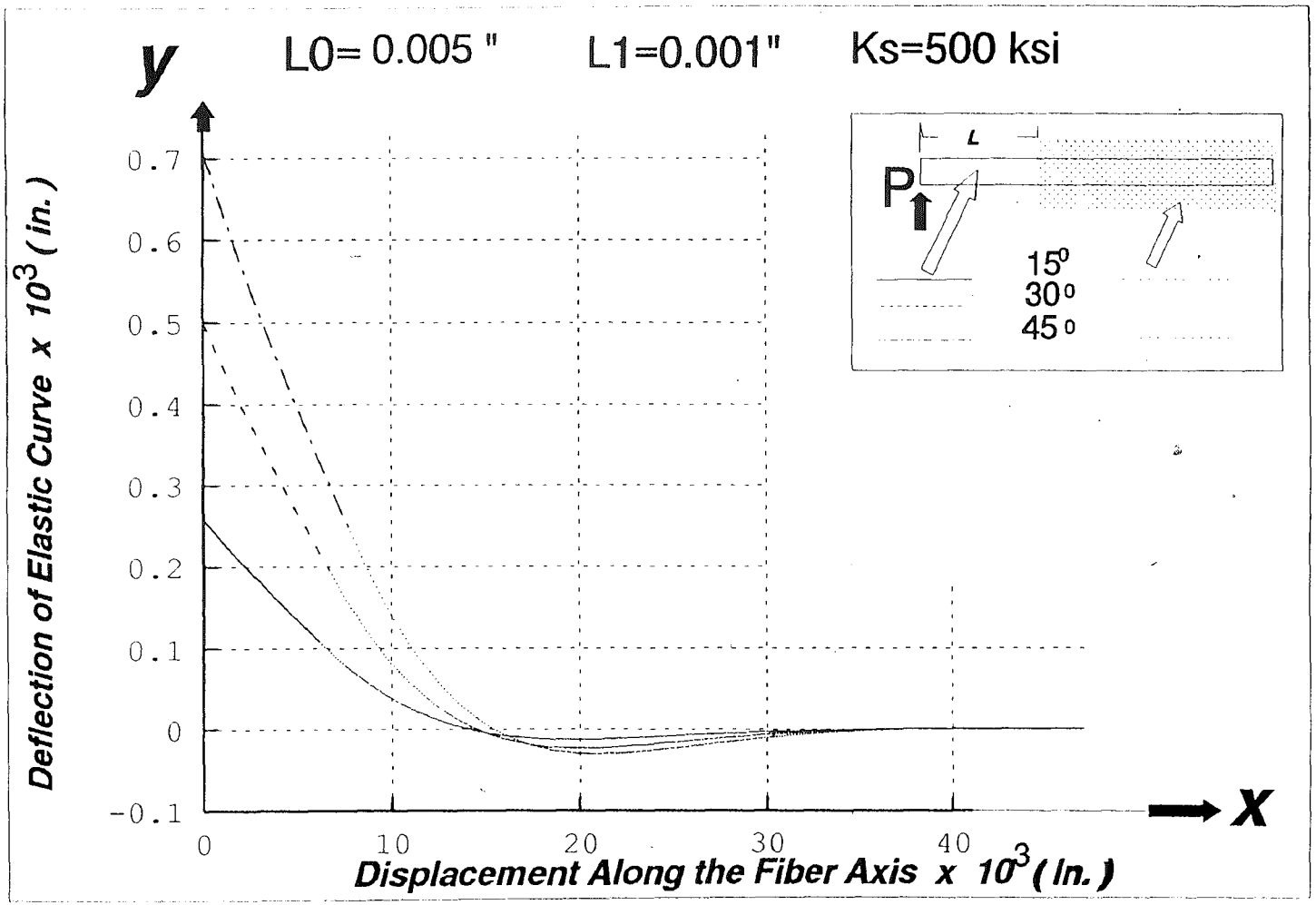

Fig. 9 - Variations in Elastic curve with Changes in Orientation Angle Θ (theoretical results)

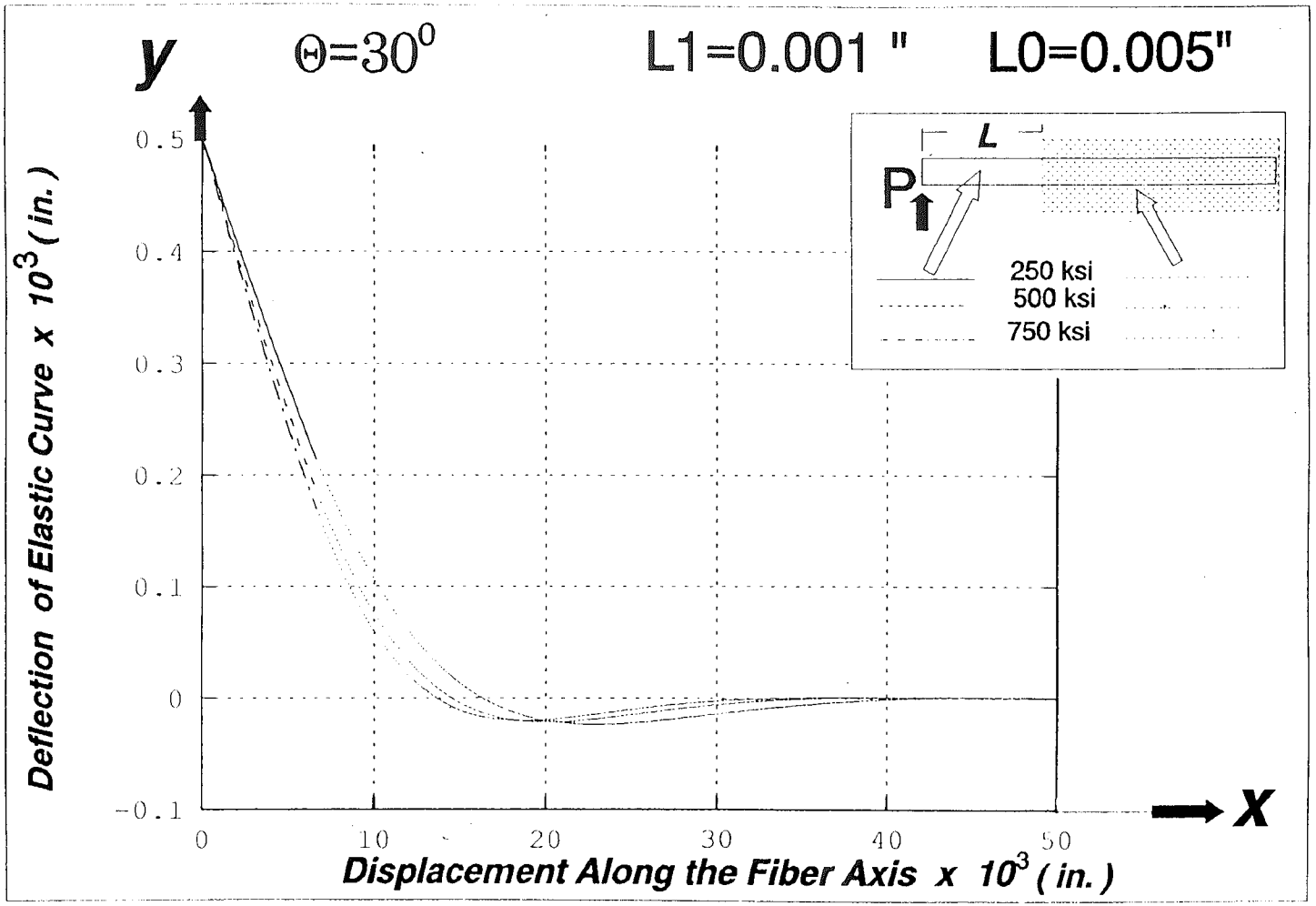

Fig. 10 - Variation of Elastic Curve with Changes in Ks (theoretical results).

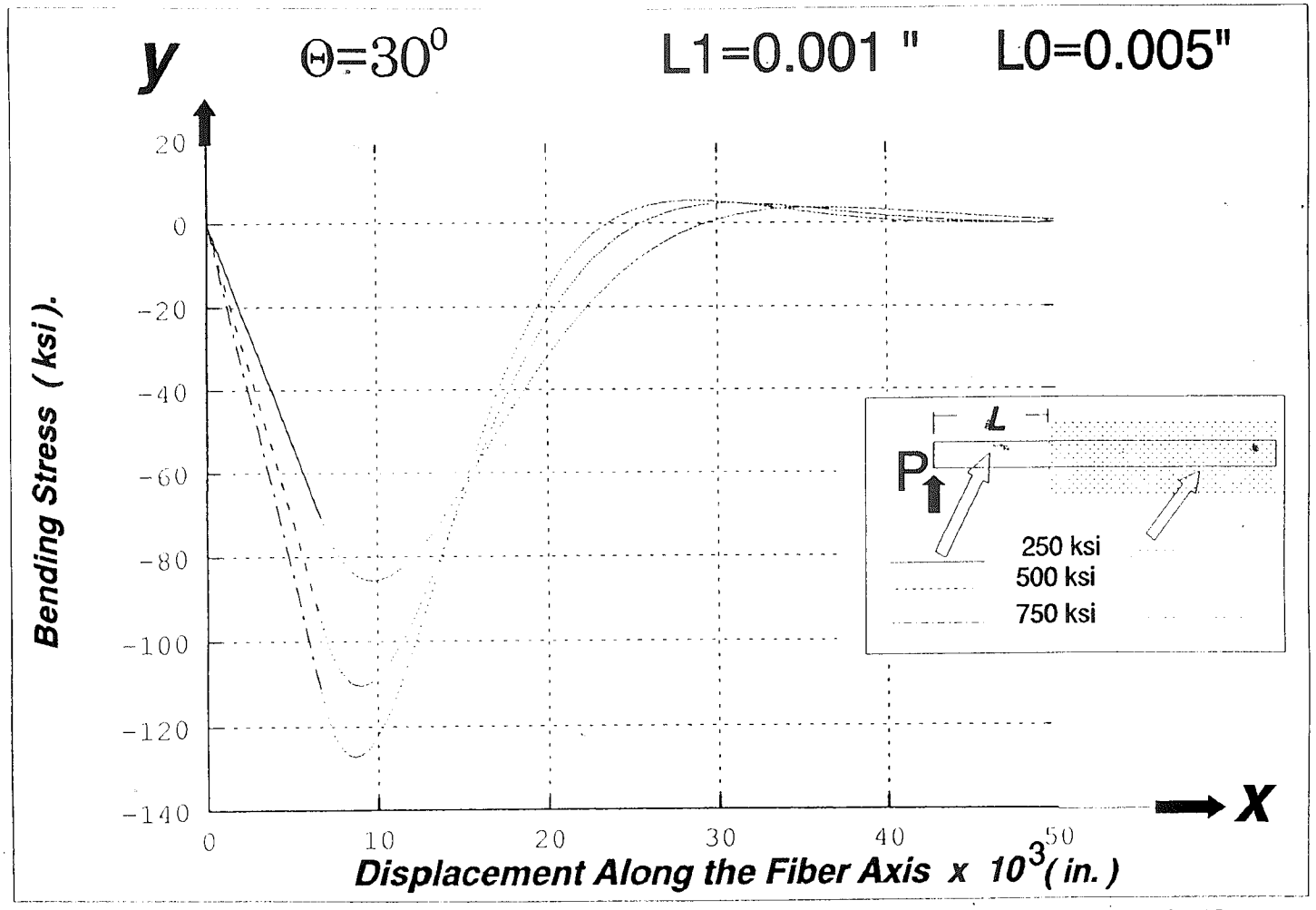

Fig. 11 - Bending Stress of partially supported semi infinite beam with changes in Ks.

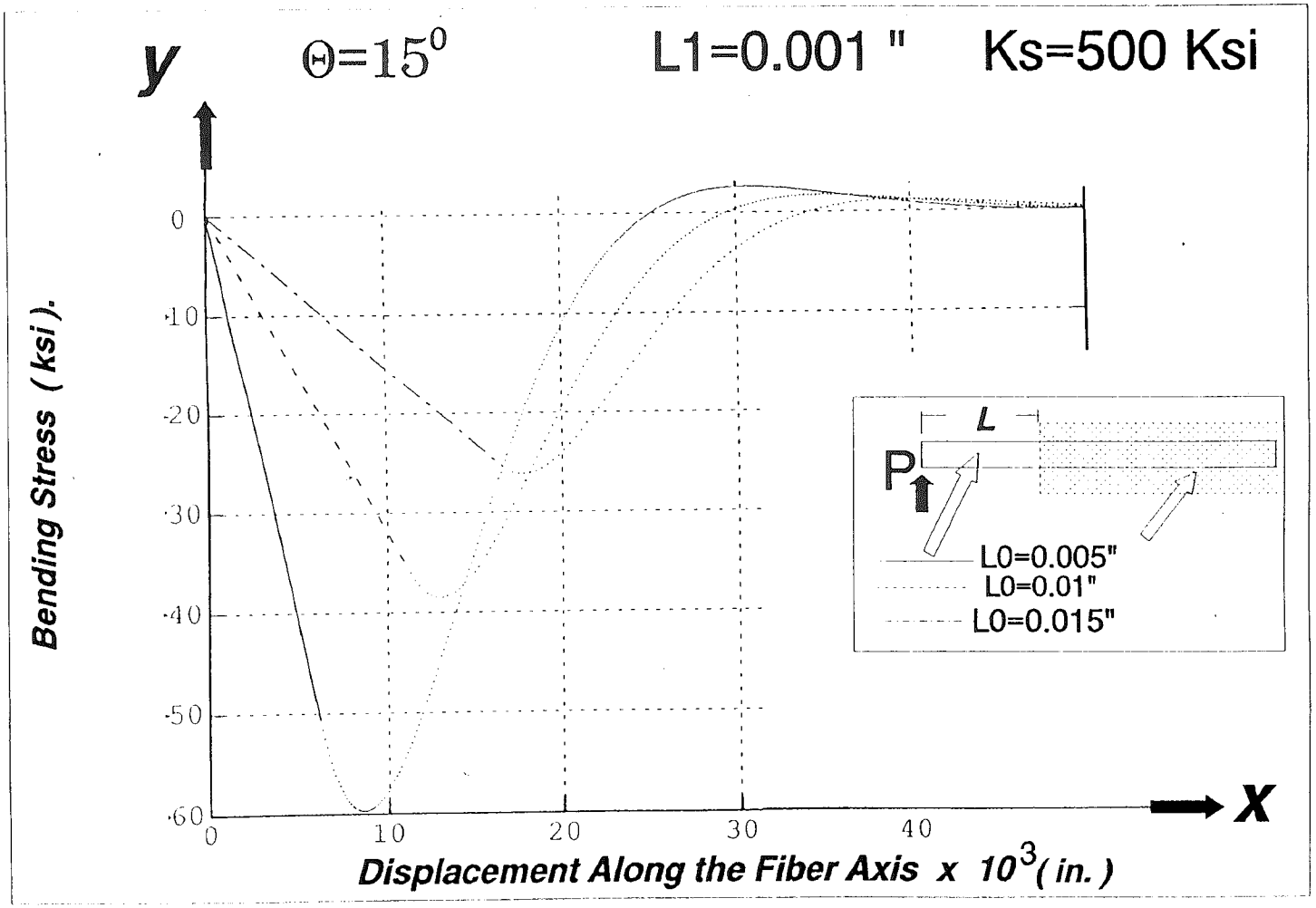

Fig. 12 - Bending Stress of partially supported semi infinite beam with changes in L0.

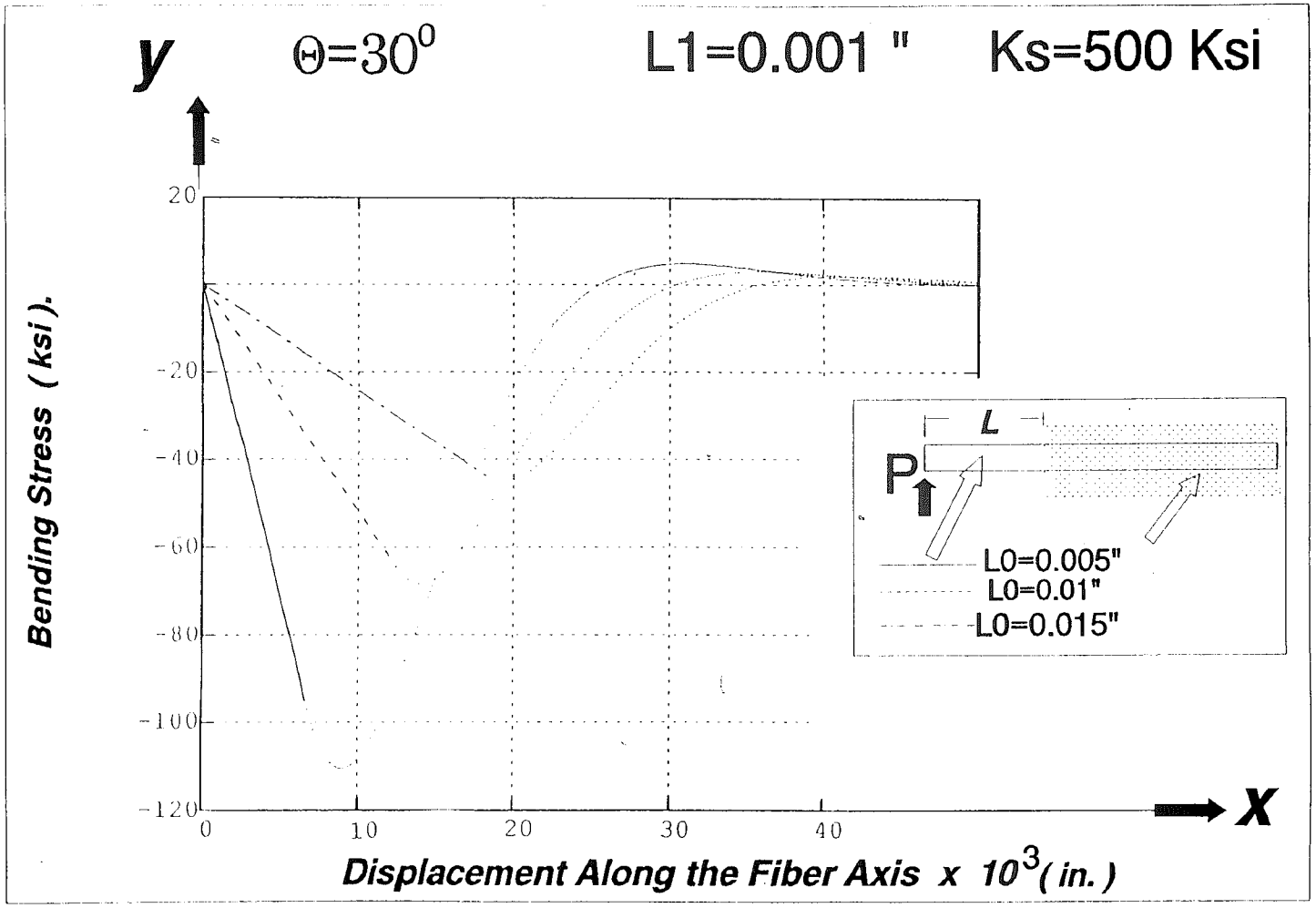

Fig. 13 - Bending Stress of partially supported semi infinite beam with changes in L0.

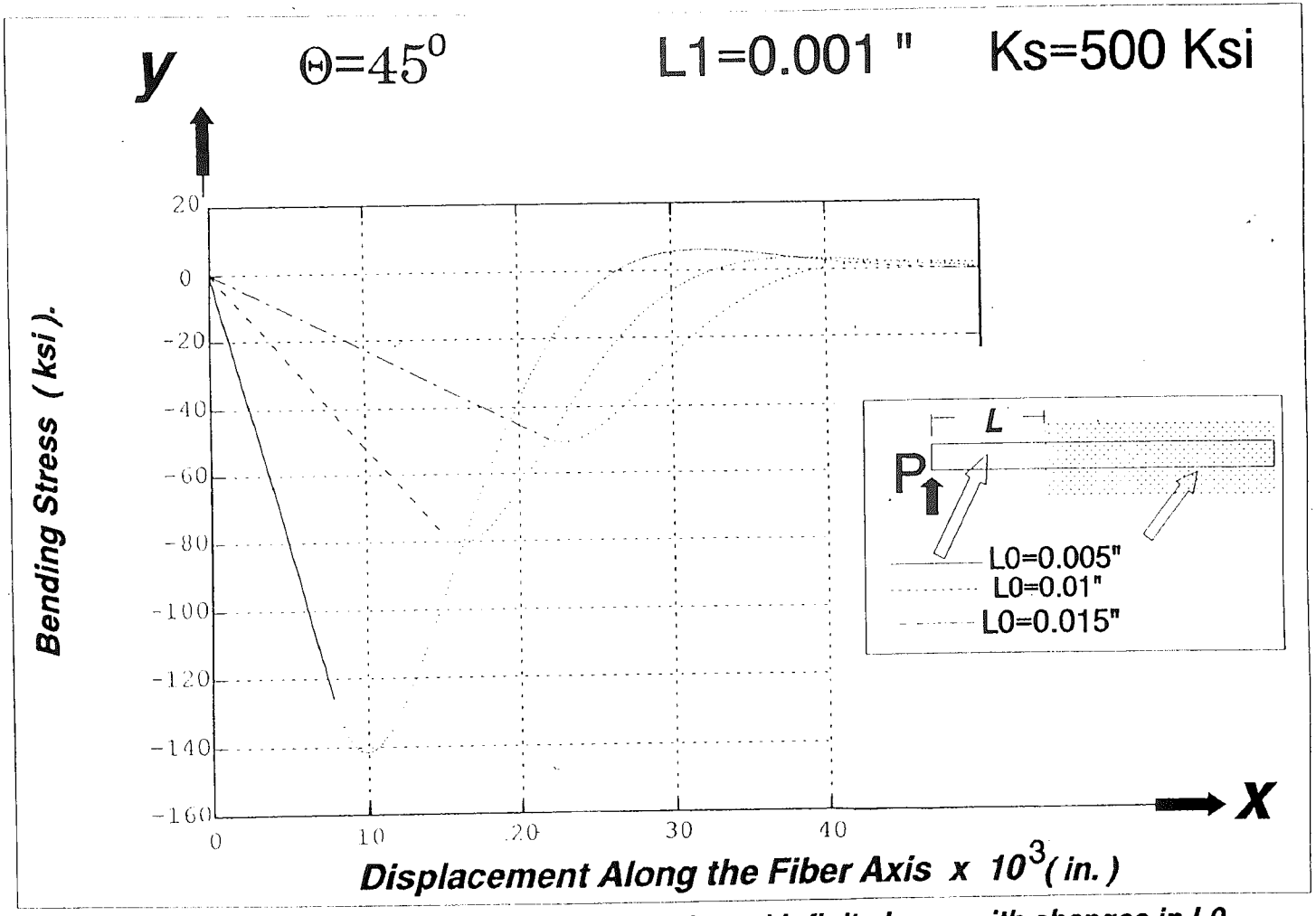

Fig. 14 - Bending Stress of partially supported semi infinite beam with changes in L0.

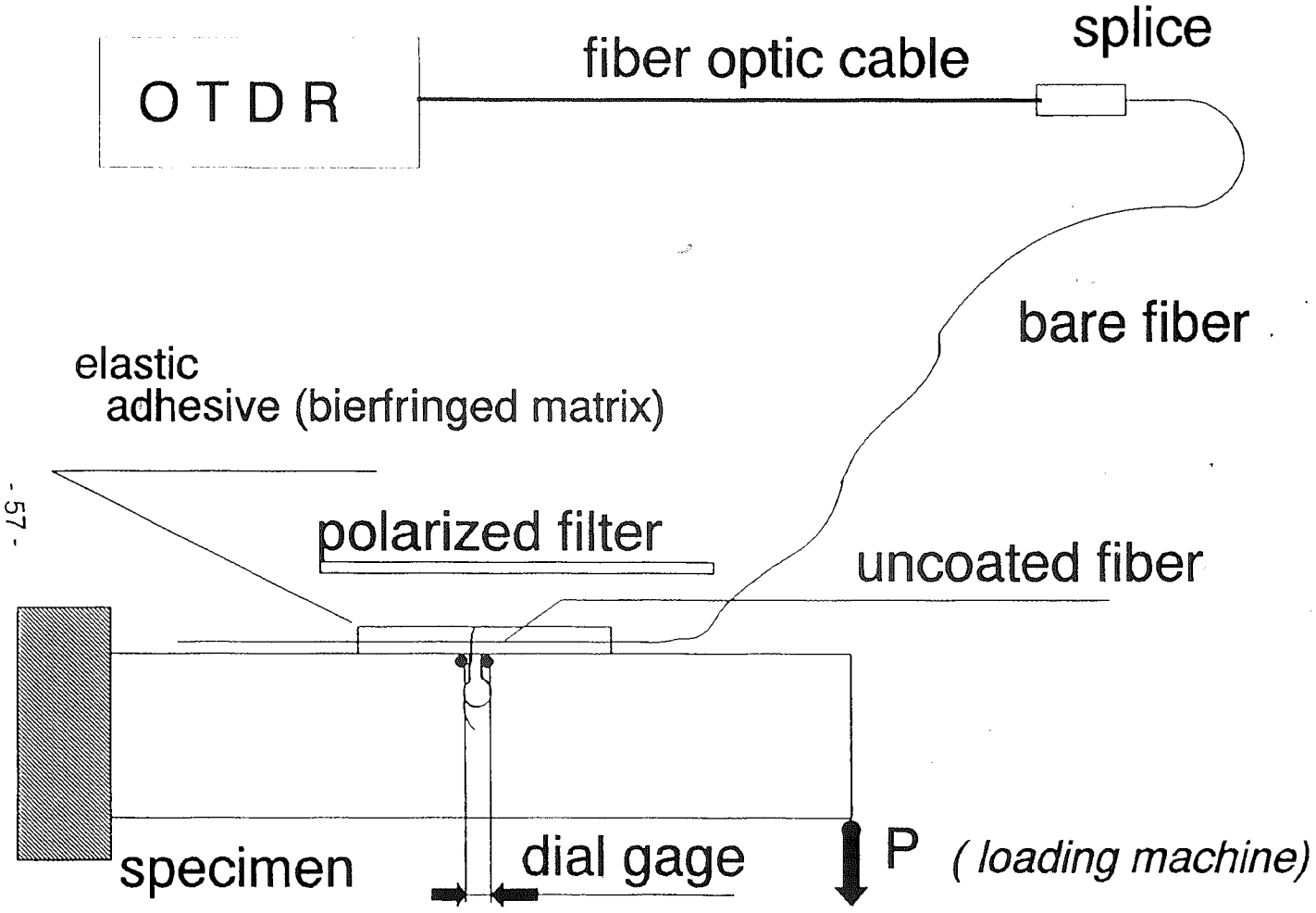

Fig. 15 - Experimental Set Up (cantilever beam specimen)

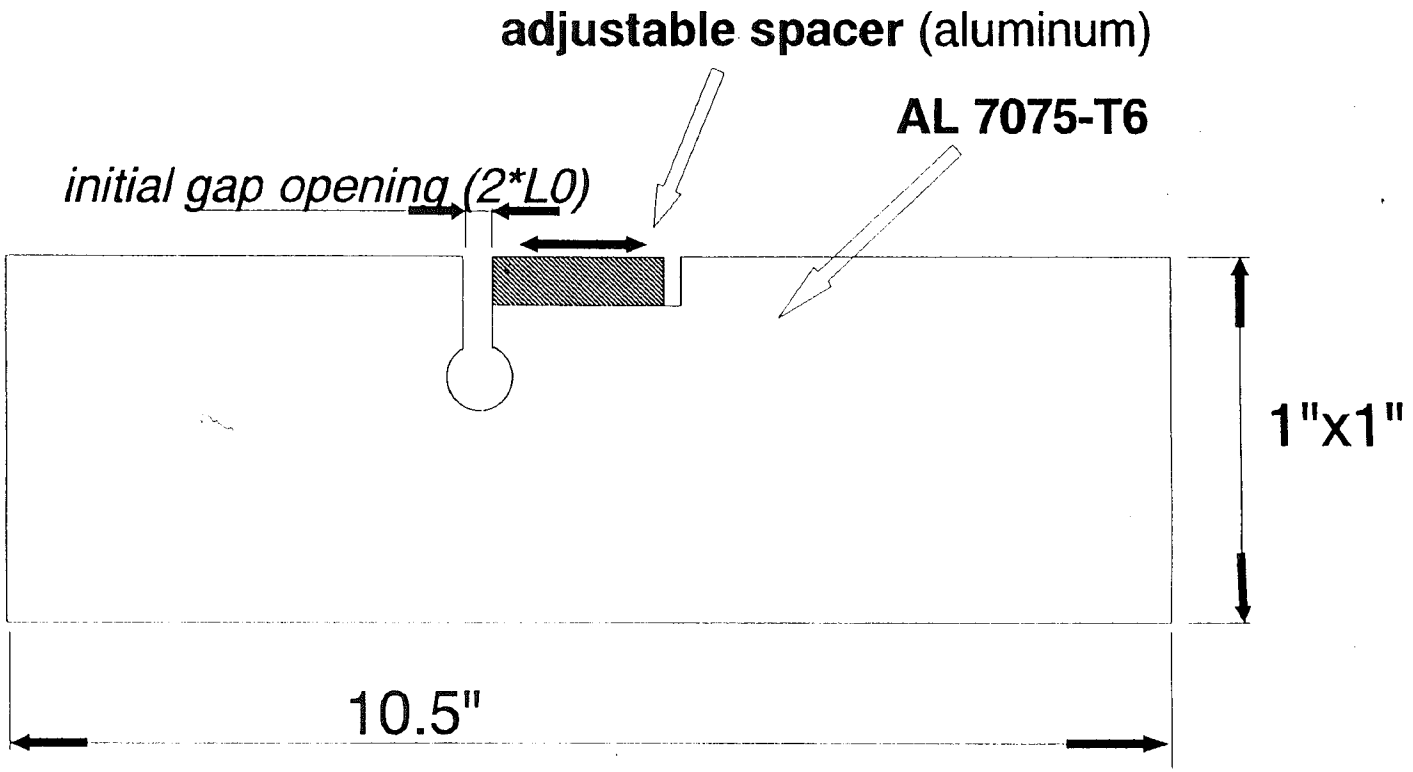

Fig. 16 - Cantilever Beam Specimen.

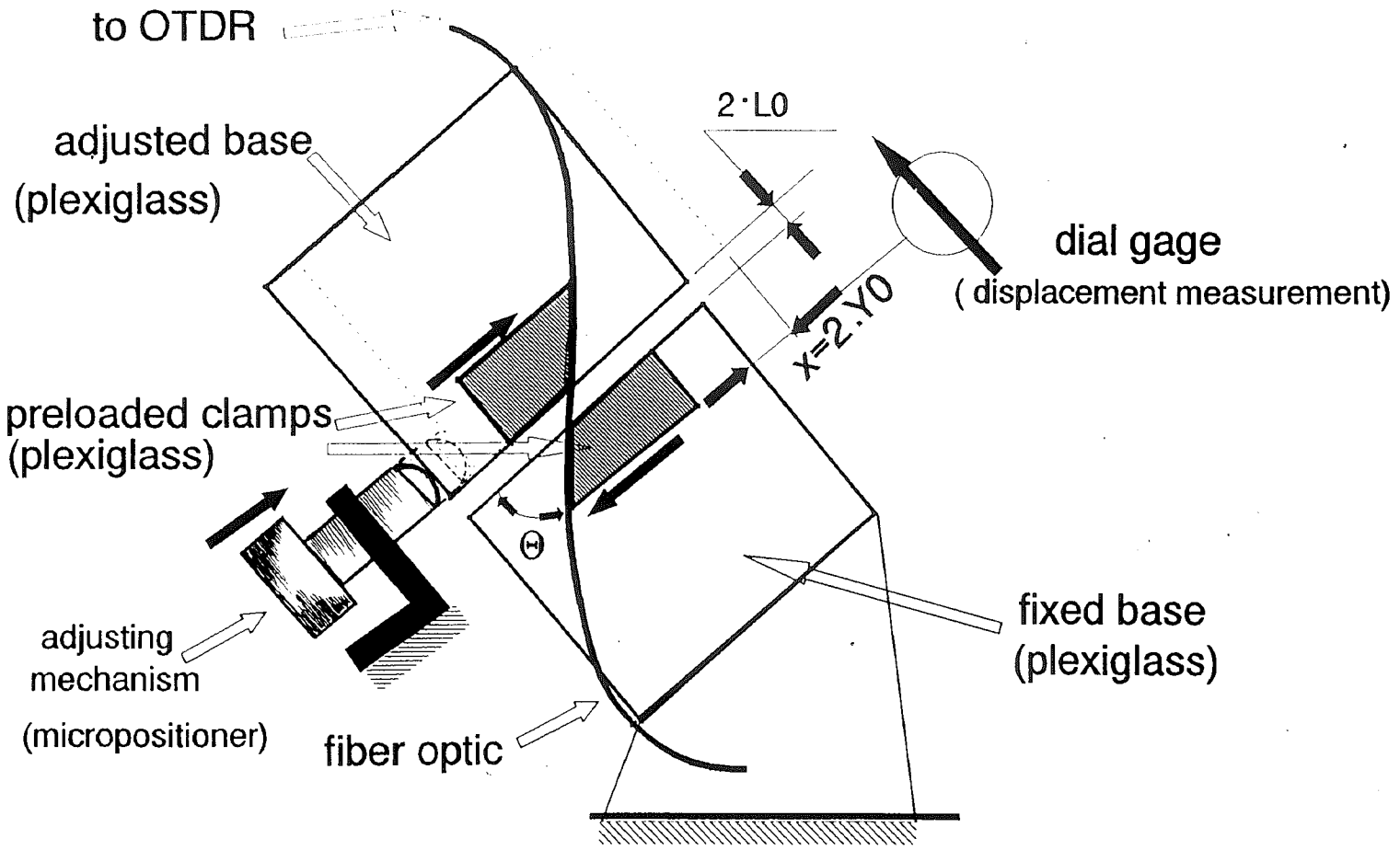

Fig. 17- Displacement Specimen

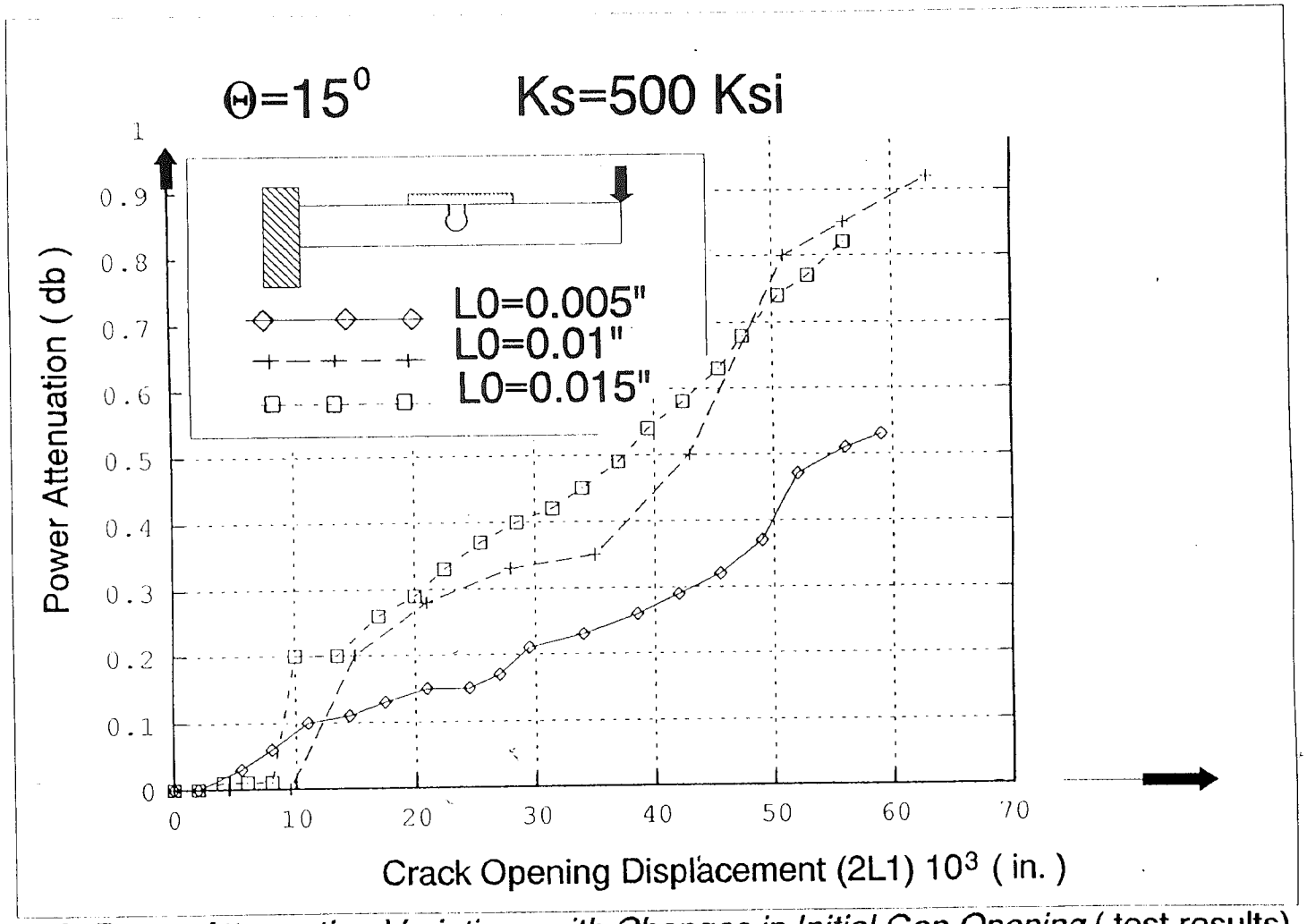

Fig. 18- Power Attenuation Variations with Changes in Initial Gap Opening (test results)
Cantilever Beam Specimen

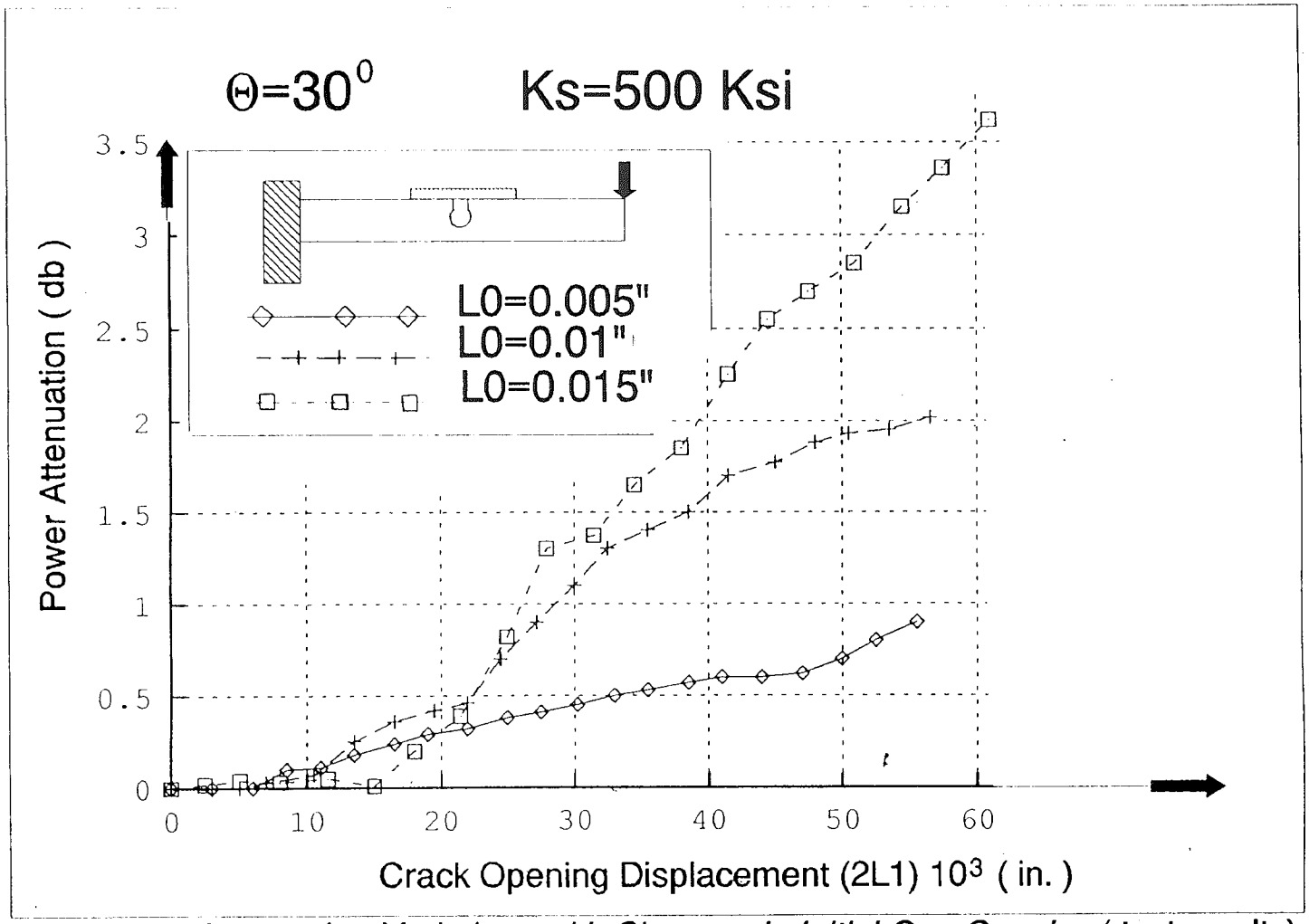

Fig. 19- Power Attenuation Variations with Changes in Initial Gap Opening (test results)
Cantilever Beam Specimen

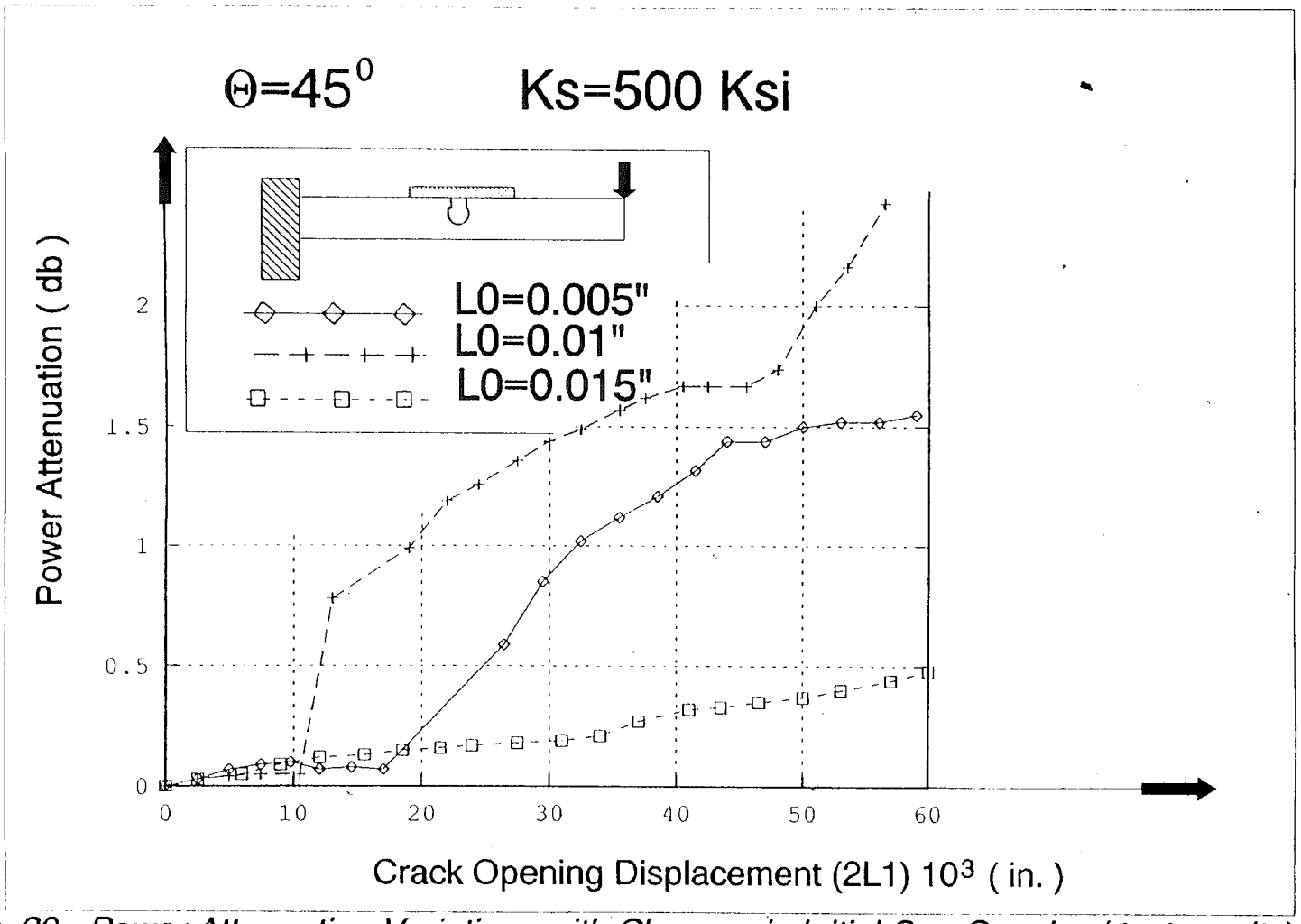

Fig. 20 - Power Attenuation Variations with Changes in Initial Gap Opening (test results)
Cantilever Beam Specimen

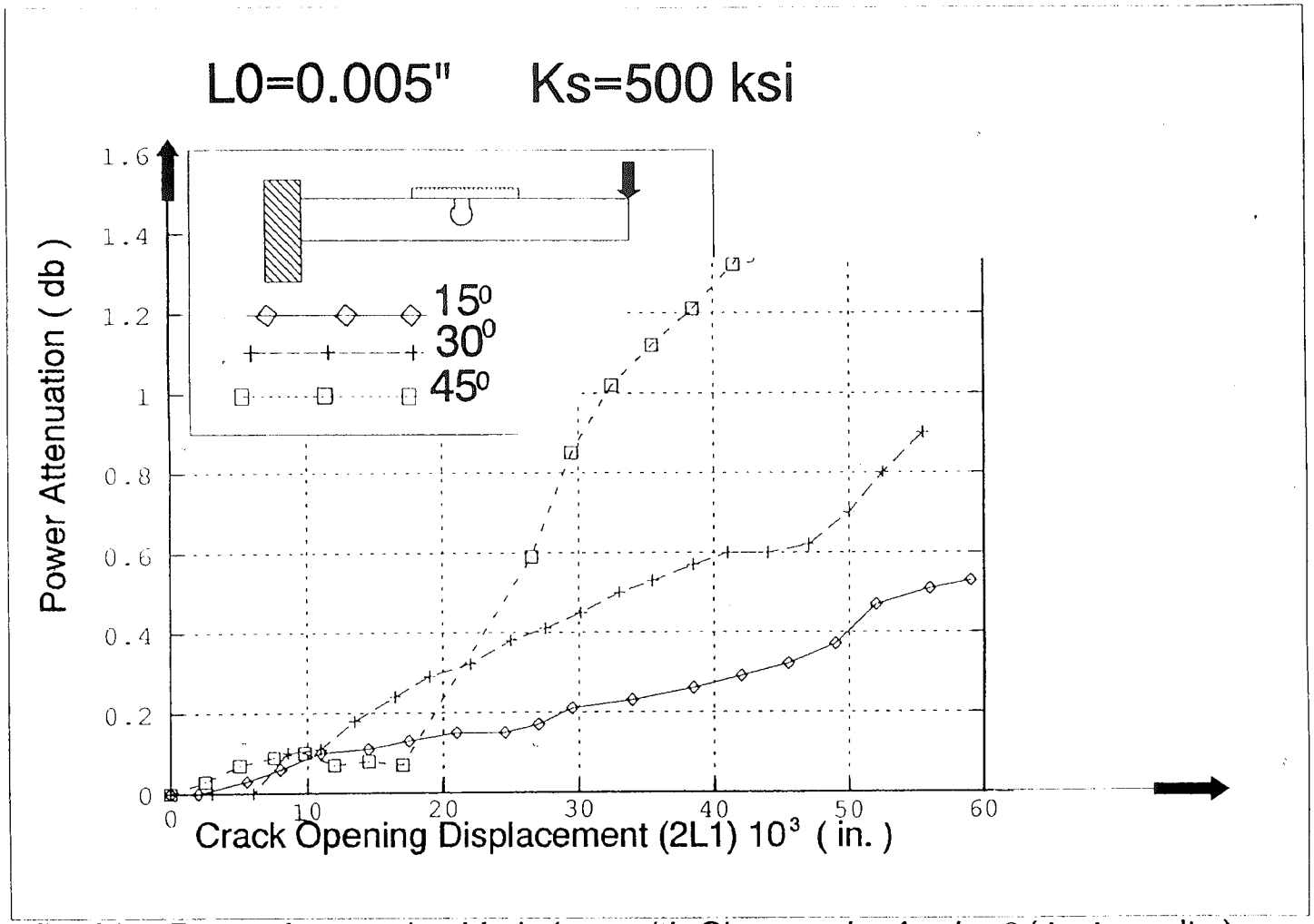

Fig. 21 - Power Attenuation Variations with Changes in Angle Θ (test results)
Cantilever Beam Specimen

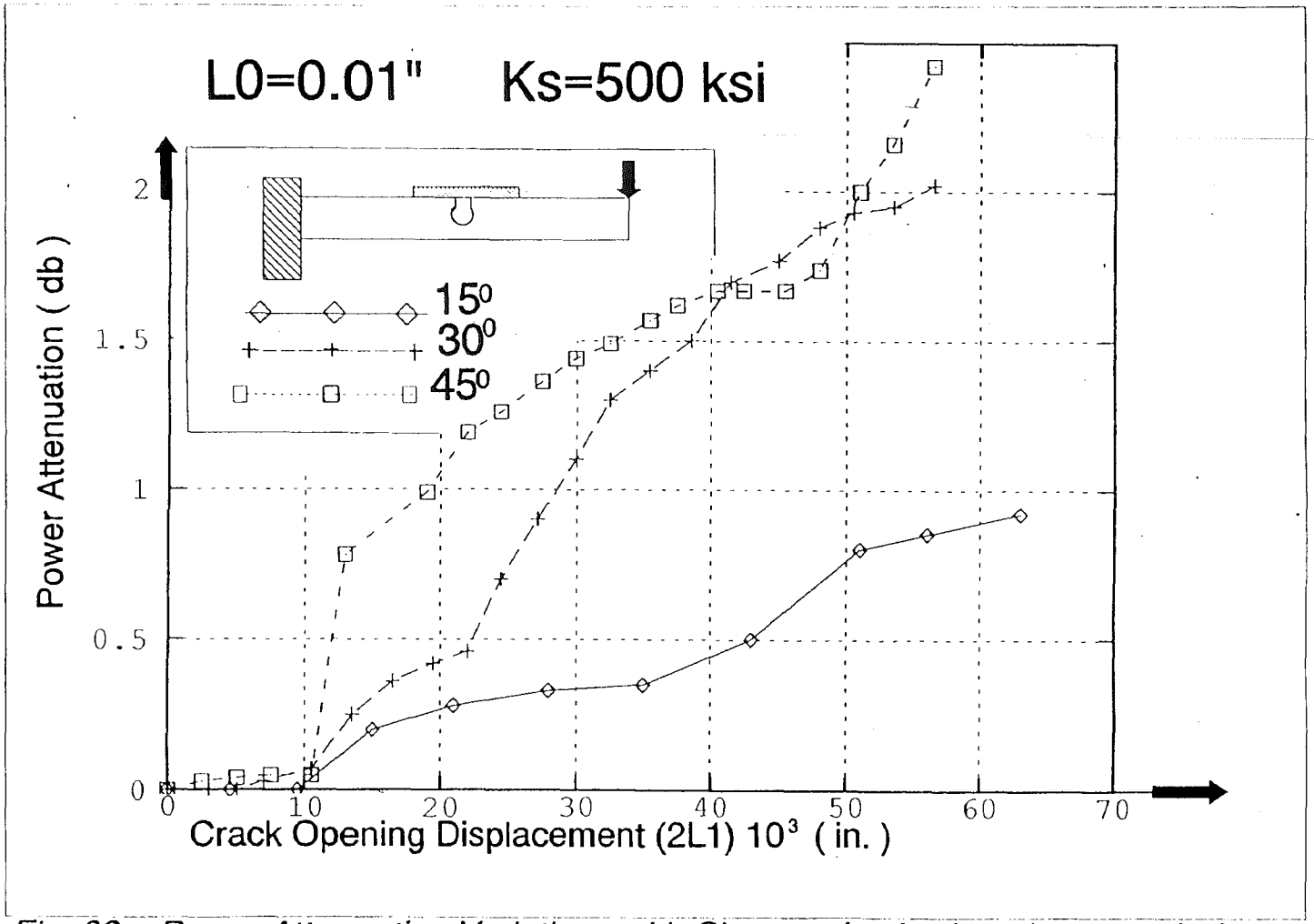

Fig. 22 - Power Attenuation Variations with Changes in Angle Θ (test results)
Cantilever Beam Specimen

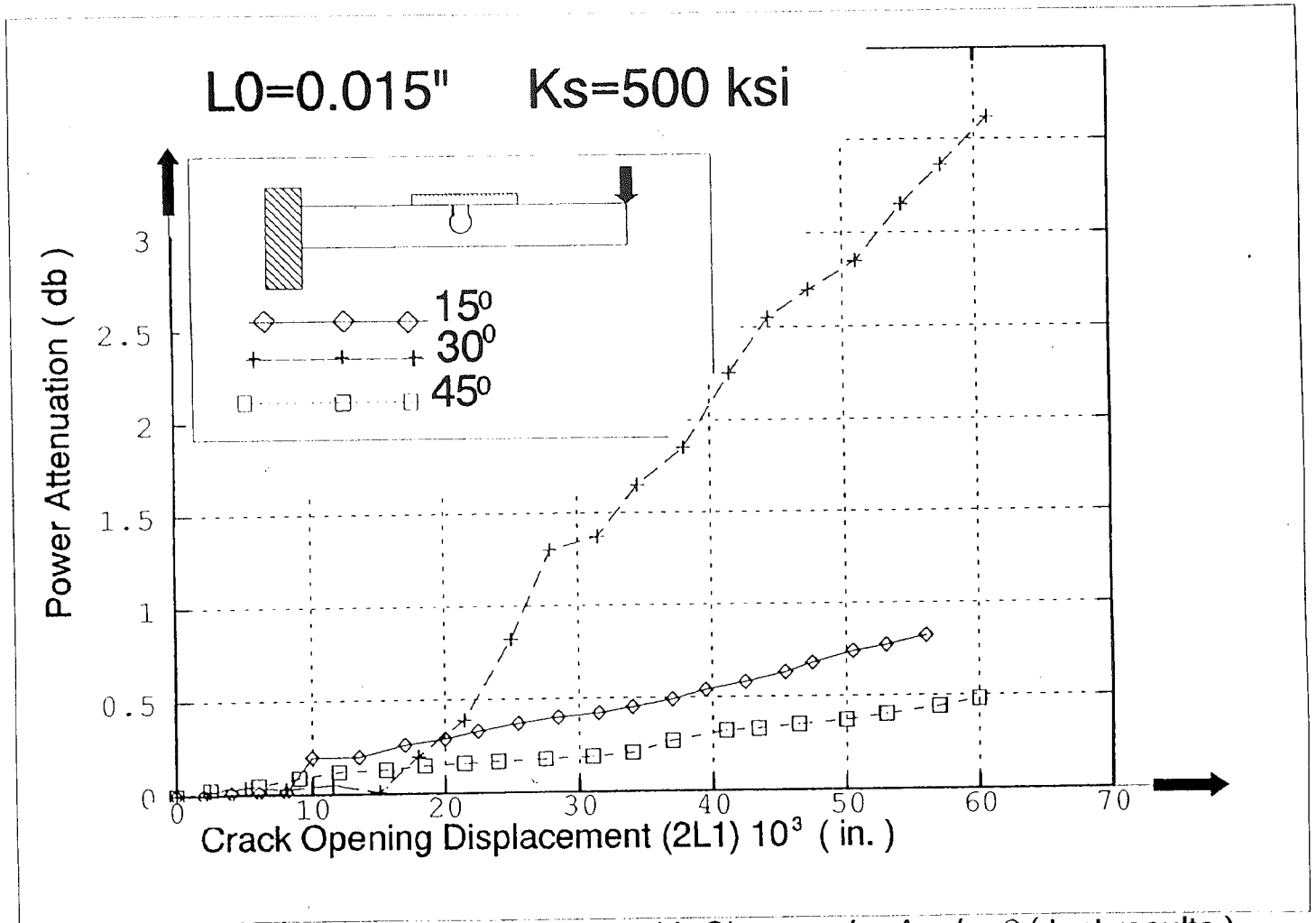

Fig. 23 - Power Attenuation Variations with Changes in Angle Θ (test results)
Cantilever Beam Specimen

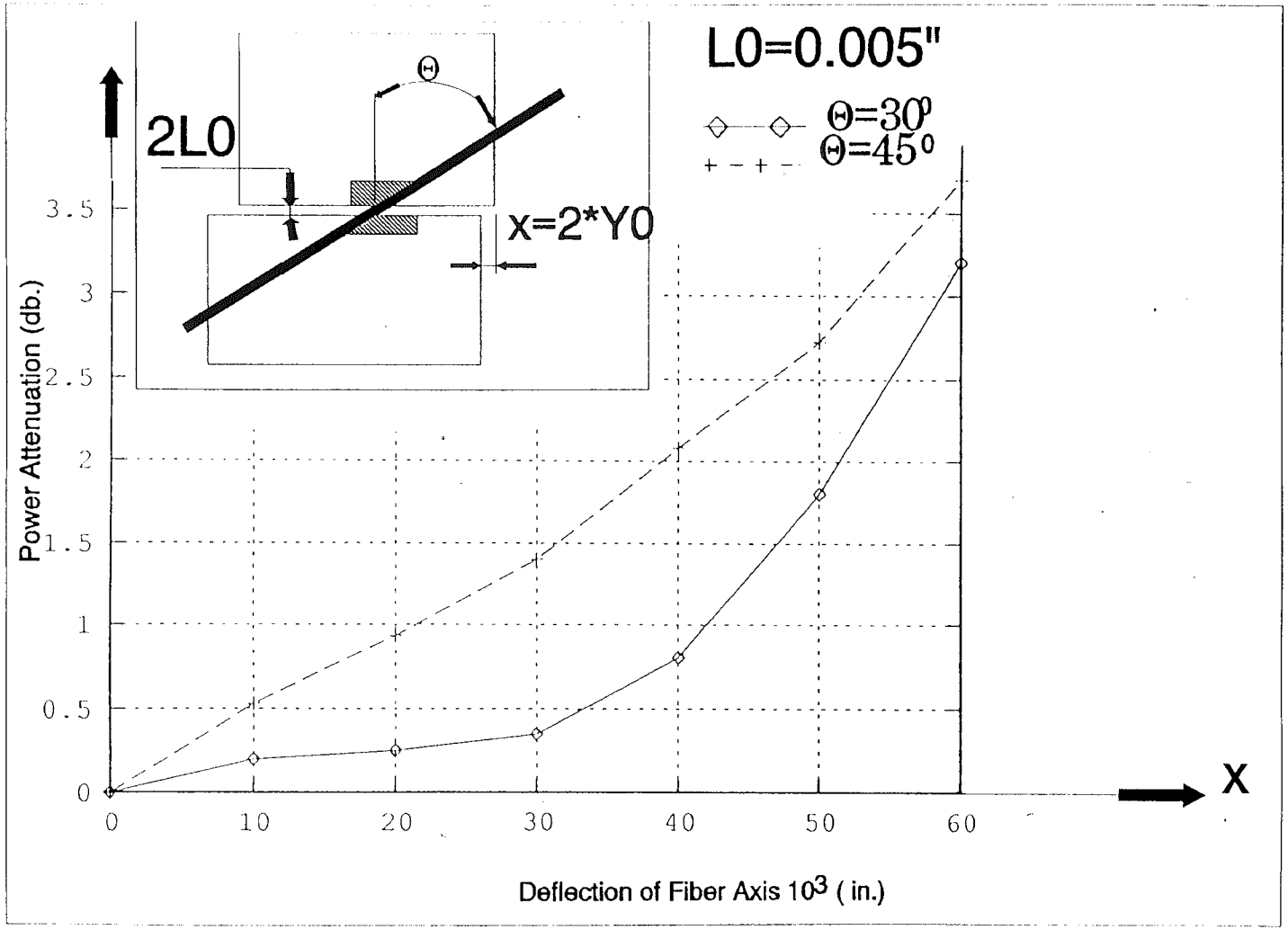

Fig. 24- Power Attenuation Variations with Changes of Θ
Displacement Specimen (test results)

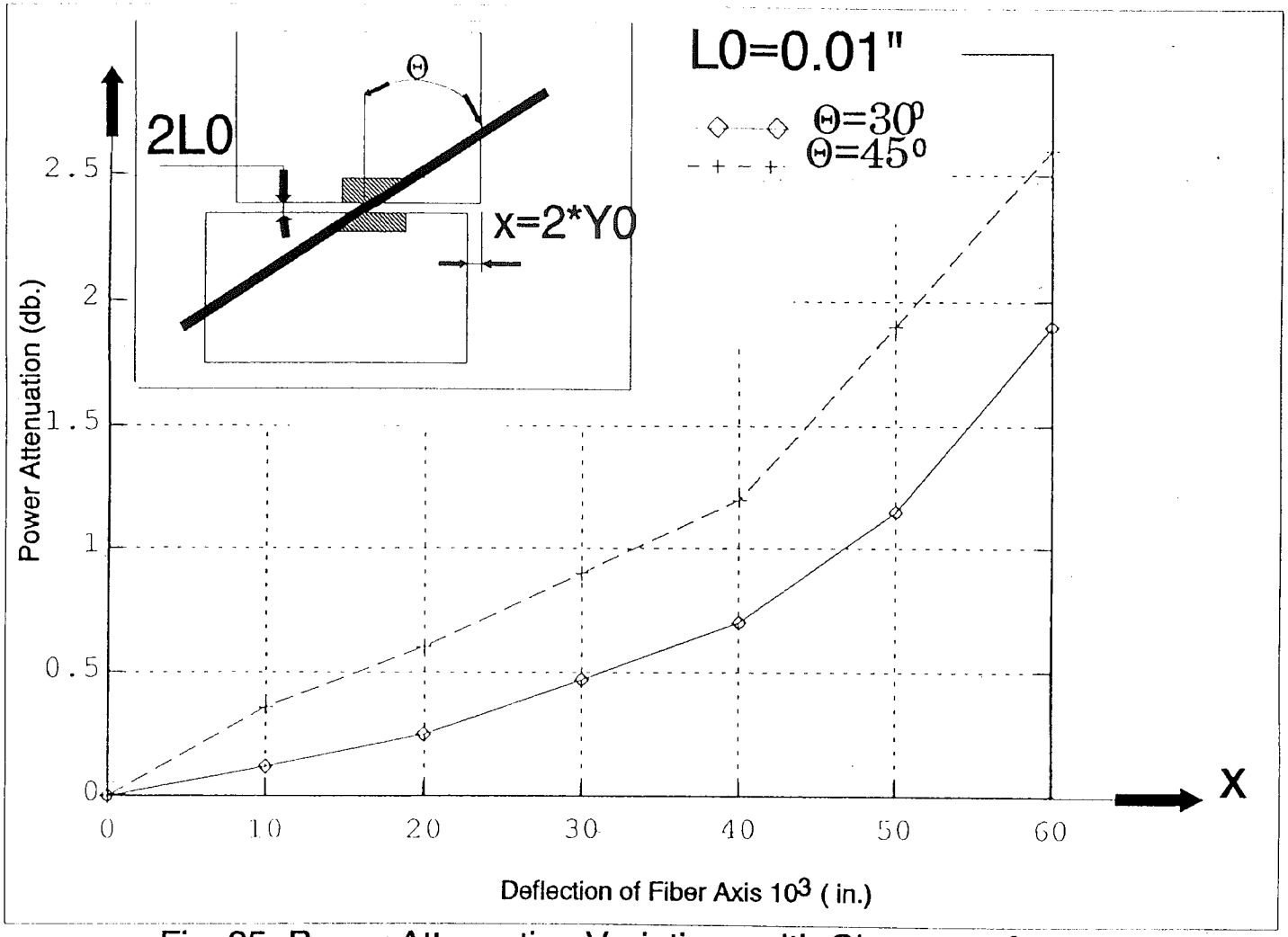

Fig. 25- Power Attenuation Variations with Changes of Θ
Displacement Specimen (test results)

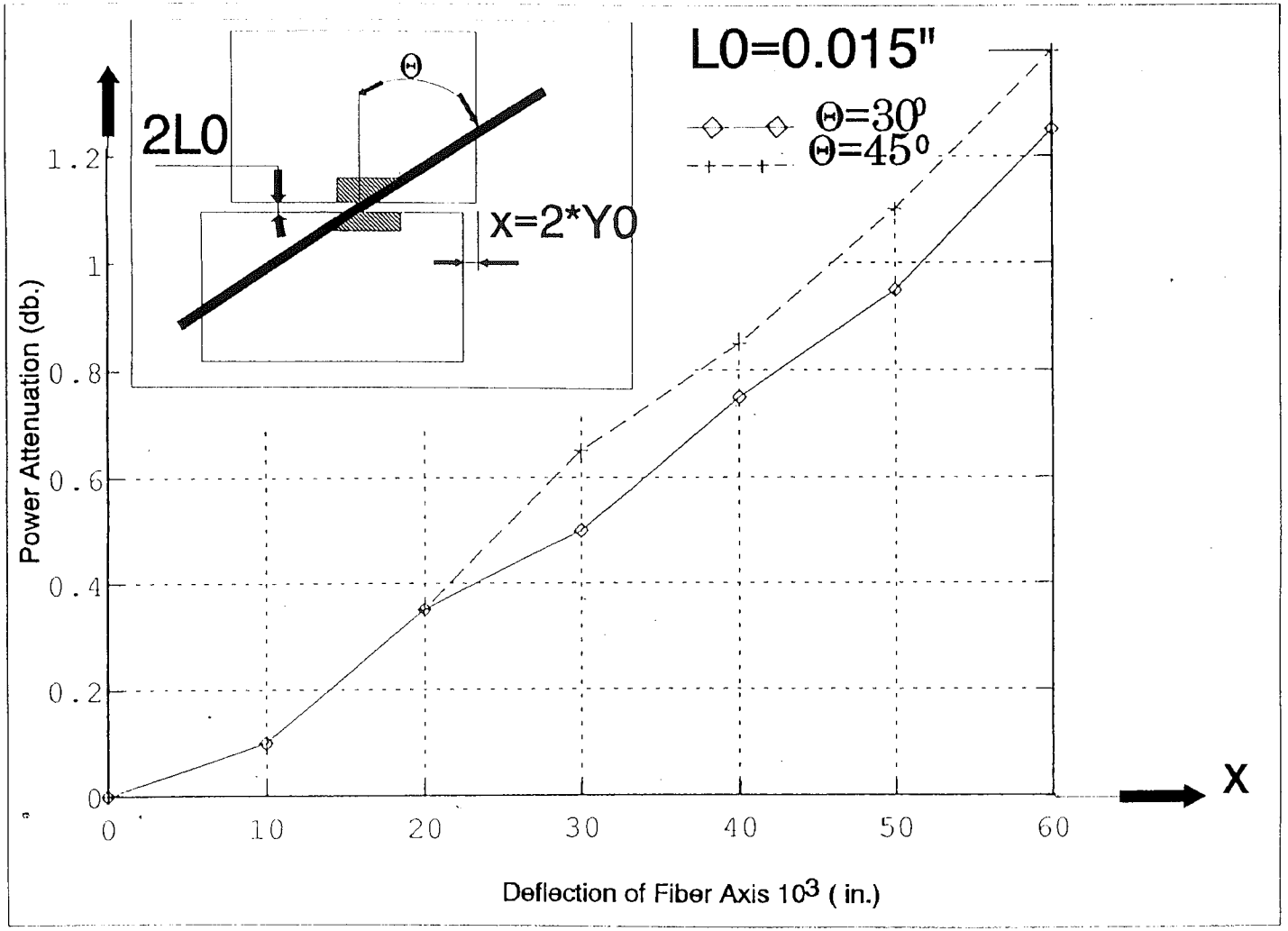

Fig. 26- Power Attenuation Variations with Changes of Θ
Displacement Specimen (test results)

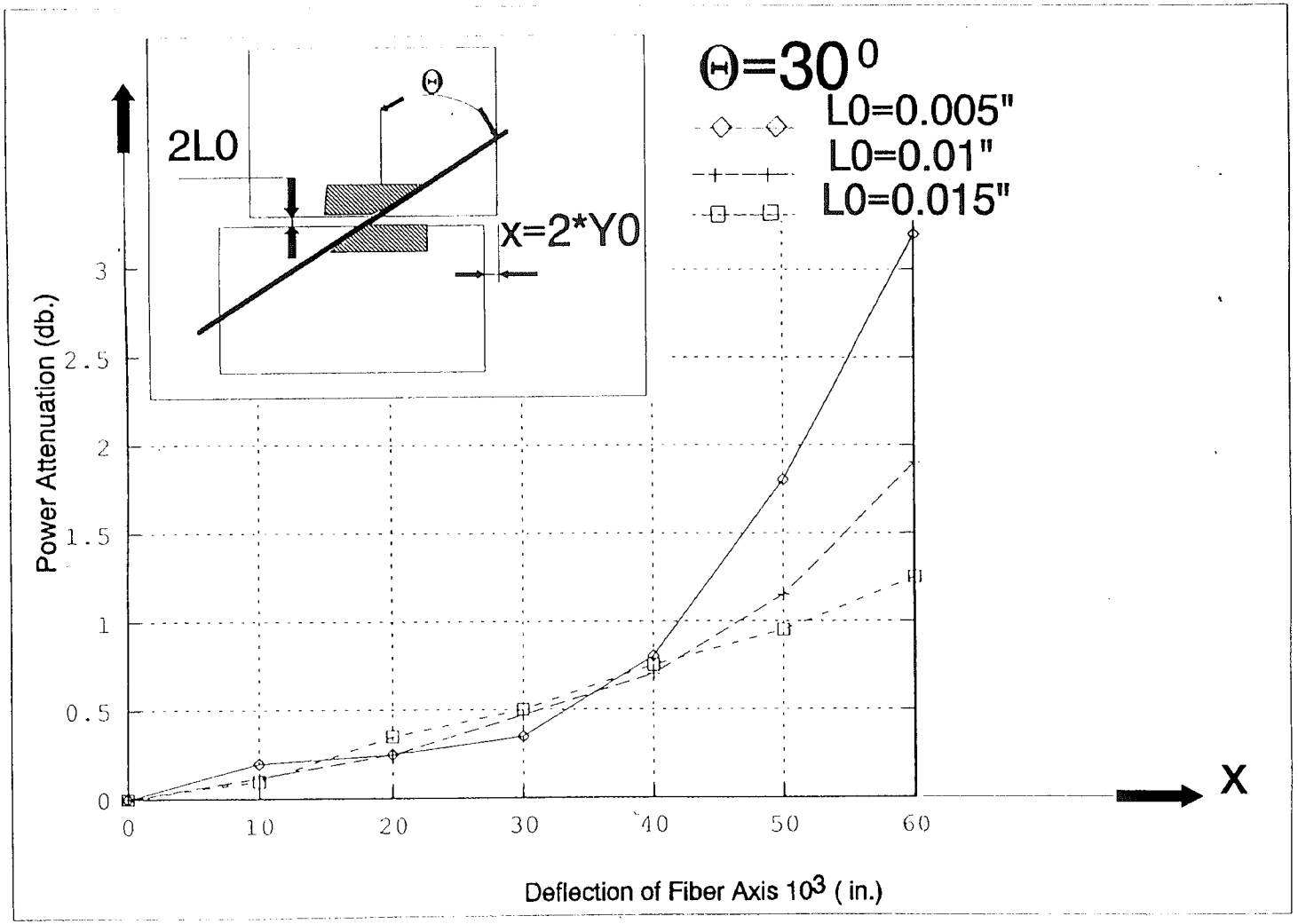

Fig. 27- Power Attenuation Variations with Changes of L0.
Displacement Specimen (test results)

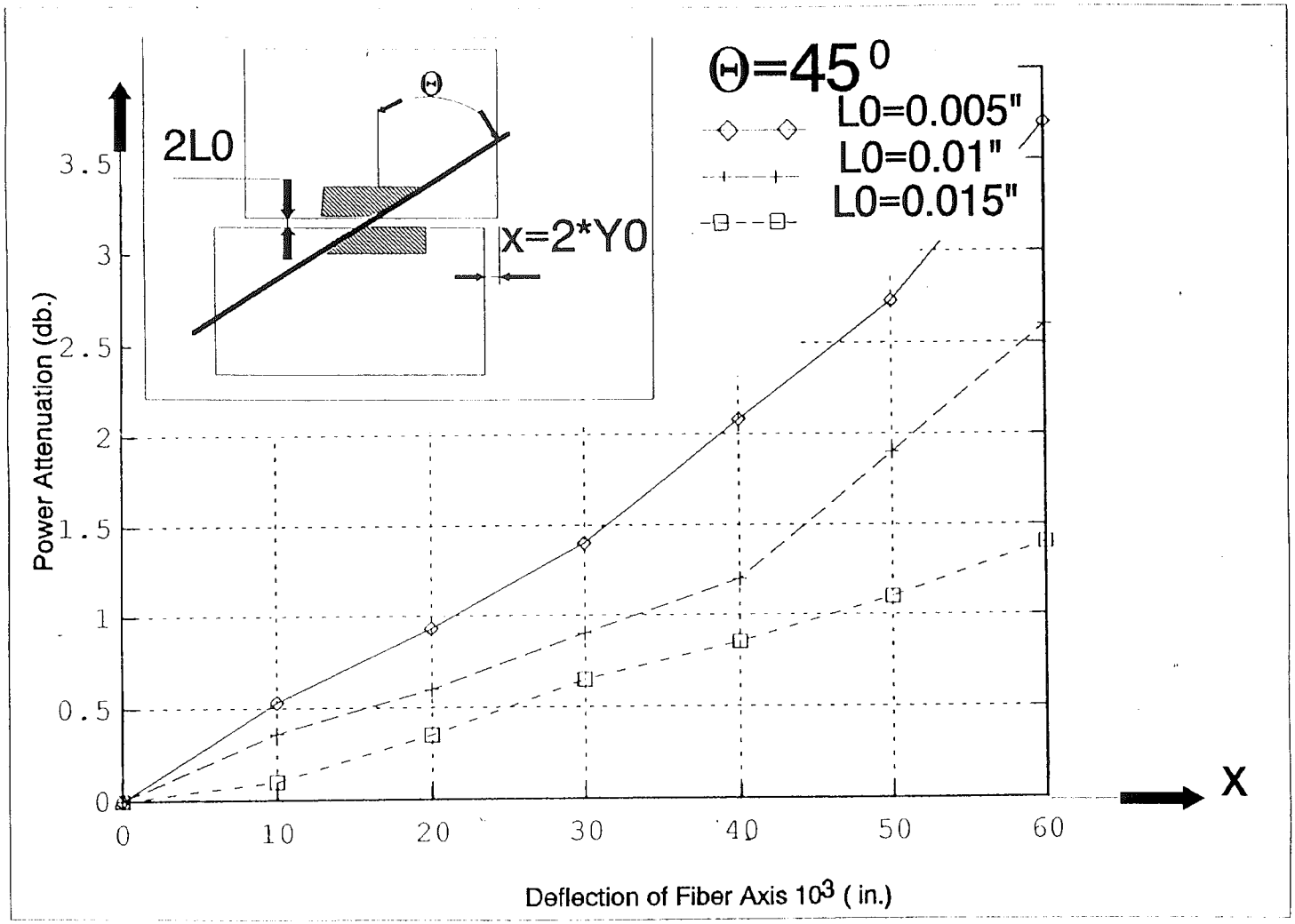

Fig. 28- Power Attenuation Variations with Changes of L0.
Displacement Specimen (test results)

LIST OF REFERENCES

1. Culshaw, B. and Dakin, J., "Optical Fiber Sensors – System and Applications", Volume 2, Norwood, MA., Artech House, Inc., 1989.

2. Hale, K.F., "Optical Fiber Sensors for Inspection Monitoring", The Institute of Physics, Vol. 15 (1984), pp. 129–135.

3. Dally, W. James & Riley, F.W., "Experimental Stress Analysis", New York (1978), McGraw–Hill Book Company.

4. Miller, M.C., "Optical Fiber Splices and Connectors, Theory and Methods", AT&T Bell Laboratories, New York, Marcel Dekker, Inc., 1986.

5. Culshaw, B. and Dakin, J., "Optical Fiber Sensors – Principles and Components", Vol. 1, Norwood, MA, Artech House, Inc., 1989.

6. Photodyne 3M 5400 OTDR Manual.

7. Love, J.D. and Winkler, C., "Power Attenuation in Bent Multimode Graded Index Slab and Fiber Waveguide", Electronic Letters, Vol. 14, No. 2 (1978),

pp. 32-34.

8. Diemeer, M.B.J. and Trommel, E.S., "Fiber Optic Microbending Sensors Sensitivity as a Function of Distortion Wavelength", Optic Letters, Vol. 9, No. 6, June 1984, pp. 260-262.

9. Defornel, F. and Arnaud, J., "Microbending Effects on Monomode Light Propogation in Multimode Fiber", Optical Society of America, Vol. 73, No. 5 (May 1983), pp. 661-668.

10. Weiss, Jonathan, D., "Fiber-Optic Strain Gauge", Journal of Lightwave Technology, Vol. 7, No. 9, Sept. 1989.

11. Asawa, C.K., Yao, S.K., Stearns, R.C., Mota, N.L., and Downs, J.W., "High Sensitivity Fiber-Optic Strain Sensors for Measuring Structural Distortion", Electronic Letters, 29th April, 1982, Vol. 18, No. 9.

12. Zimmermann, Bernard D., Claus, R.O., Kapp, D.A., and Murphy, K.A., "Fiber Optic Sensors Using High-Resolution Optical Time Domain Instrumentation System", Journal of Lightwave Technology, Vol. 8, No. 9, September 1990.

13. Beheim, Glenn, Anthan, Donald J., "Loss Compensation of Intensity – Modulation Fiber–Optic Sensors", NASA Technical Memorandum 88825, Fiber Optic and Lasers IV. The Society of Photo–Optical Instrumentation Engineers, Cambridge, Massachusetts, September 21–26, 1986.

14. Leka, G. Lawrence and Bayo, Eduardo, "A Close Loop at the Embedment of Optical Fibers into Composite Structures", Journal of Composites, Technology & Research, 1989, pp. 106–112.

15. Morton, J., and Groves, G.W., "The Cracking of Composites Consisting of Discontinuous Ductile Fibers in a Brittle Matrix – Effect of Fiber Orientation", Journal of Material Science, 9 (1974), pp. 1436–1445.

16. Stucke, M.S., and Majumdar, A.J., "Microstructure of Glass Fiber–Reinforced Cement Composites", Journal of Material Science, 11 (1976), pp. 1019–1030.

17. Aveston, J., Mercer, R.A., Sillwood, J.N., "Fiber Reinforced Cements – Scientific Foundation for Specifications", Composites, Standards, Testing and Design, 1976, pp. 93–103.

18. Hetenyi, M., "Beams on Elastic Foundation", Ann Arbor (1946), The

University of Michigan Press.

19. Bentur, A., "Fiber Reinforced Cementitious Composites", New York (1990), Elsvier Applied Science.

20. Ritter, J.E., Helfinstine, J.D., "OVD Process Modification for Improved Optical-Fiber Strength Reliability", Corning Technical Report TR-66 March 1987.

VITA

Joram Vishlizki, son of Efraim and Pnina Vishlizki, was born in Tel-Aviv, Israel in September 1951.

In 1977 he received his B.Sc. degree in Mechanical Engineering from The Ben-Gurion University, Beer-Sheva, Israel. After graduation, he was hired by a R&D company as a research engineer. His work was involved with opto-mechanical systems and system engineering.

In September 1989 he joined the Center for Advanced Technology for Large Structural Systems at Lehigh University, as a visiting scientist and worked on fiber optic sensors for large structures.

In January 1990 he became a full-time Mechanical Engineering student, working towards his M.Sc. on the subject: "Crack Detection with Fiber Optic Sensor", and returned to Israel during the summer of 1991.

END

OF

TITLE